ACS APPLIED ENERGY MATERIALS

www.acsaem.org
Review

Substrate Designs for Stable Potassium Metal Anodes

Yupei Han and Yang Xu*

Cite This: https://doi.org/10.1021/acsaem.5c02661
Read Online

ABSTRACT: Potassium metal batteries (PMBs) are gaining attention as low-cost, sustainable, and high-energy storage. Their practical implementation, however, is impeded by instability of the potassium (K) metal anode, manifested as dendritic growth, large volume fluctuations, and fragile solid electrolyte interphases (SEIs), all of which accelerate capacity fading and safety risks. This review highlights recent advances in substrate design for stabilizing K metal anodes, categorized into five strategies: (i) three-dimensional host architectures, (ii) heteroatom doping and molecular grafting, (iii) inorganic nanoparticle incorporation, (iv) alloying seed engineering, and (v) substrate-regulated SEI formation via work function modulation. Mechanistic insights from experimental and theoretical studies are integrated with performance comparisons to evaluate trade-offs between deposition control, SEI stability, scalability, and cost. Key challenges for commercialization are outlined, including long-term cycling under practical conditions, integration with high-energy-density cathodes, and scalable fabrication. By advancing structural, chemical, and electronic design principles, PMBs can progress toward reliable, high-performance energy storage.

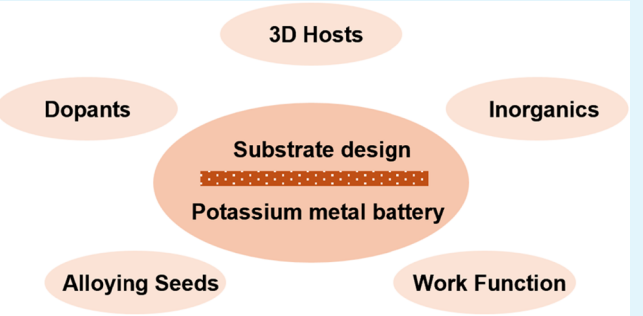

KEYWORDS: *potassium metal batteries, substrate engineering, dendrite suppression, nucleation and deposition, scalable anode design*

1. INTRODUCTION

Achieving global carbon neutrality requires not only the rapid expansion of renewable energy generation but also the deployment of efficient, reliable, and sustainable energy storage systems to balance supply demand fluctuations.[1,2] Rechargeable batteries have become a cornerstone of zero-emission technologies. Among them, lithium-ion batteries (LIBs) have achieved widespread adoption in electric transportation, portable electronics, unmanned aerial vehicles, and robotics, owing to their high energy density, low self-discharge rate, and long cycle life.[3] However, both the cathode and anode capacities in LIBs are approaching their theoretical limits, hindering progress toward achieving the target energy density of 500 Wh kg^{-1}.[4]

Lithium metal batteries (LMBs), which employ energy-dense lithium (Li) metal anodes, offer a promising route to reach this benchmark at the device level, including packaging.[5,6] Nevertheless, the scarcity of Li in the upper crust (0.002 wt %),[7] uneven geographical distribution,[8] and the surging demand from battery production (~87% of global Li consumption),[9] raise concerns over long-term resource availability.[10] Pronounced price volatility and high resource costs (~10^4 $ per metric ton)[9] further restrict their suitability for large-scale, cost-sensitive applications such as grid-level storage.

To meet net-zero targets, next-generation rechargeable battery chemistries must combine high performance with the use of earth-abundant, low-cost materials.[11,12] Inexpensive sodium- and potassium-ion batteries are attracting increasing attention.[13−15] To further enhance energy density, potassium metal batteries (PMBs) have recently emerged as a promising contender, owing to potassium (K)'s upper-crustal abundance (2.32 wt %, over 1000 times that of Li),[7] wide geographic availability, low resource cost (~10^3 $ per metric ton, one-tenth that of Li, Figure 1A),[9] and favorable electrochemical properties.[16,17]

Electrochemically, the K^+/K redox couple exhibits a standard potential of −2.93 V versus the standard hydrogen electrode (SHE), lower than that of sodium (−2.71 V for Na^+/Na), and in propylene carbonate (PC) it is 0.09 and 0.32 V lower than that of Li^+/Li and Na^+/Na, respectively (Figure 1B).[18] These attributes, combined with the high theoretical specific capacity of K metal anode (687 mAh g^{-1}), enable high-voltage, energy-dense cell designs. In addition, potassium's weaker Lewis acidity yields a smaller solvated ion radius than Li or Na, resulting in enhanced ionic conductivity in K

Received: August 23, 2025
Revised: October 15, 2025
Accepted: October 17, 2025

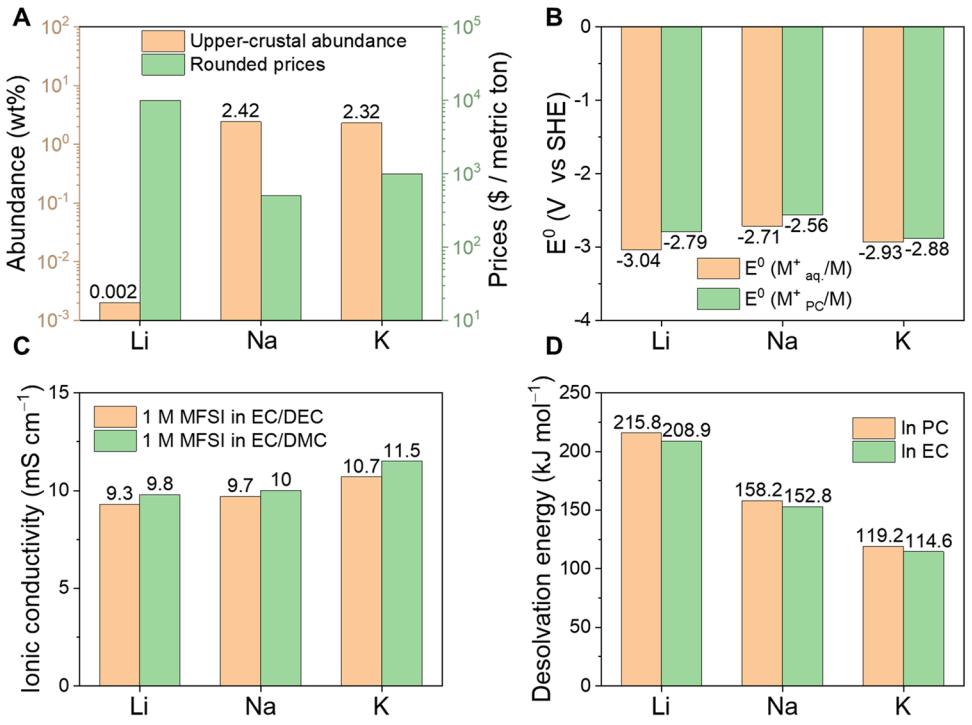

Figure 1. Resource abundances, market prices, and electrochemical properties of Li, Na, and K systems. Aq.—aqueous; M—mol; PC—propylene carbonate; EC—ethylene carbonate; DEC—diethyl carbonate; and DMC—dimethyl carbonate. (A) Upper-crustal abundance and approximate market prices of Li, Na, and K resources. Abundance values are based on recommended compositions of the upper continental crust, where Na and K abundances are derived from Na_2O and K_2O values.[7] Prices represent annual averages defined by USGS standards (2025)[9] and may fluctuate significantly: Li, contract average of lithium carbonate or lithium hydroxide; Na, average price of soda ash or table salt; K, K_2O-equivalent or muriate of potash spot average. (B) Standard redox potentials (E^0) of Li^+/Li, Na^+/Na, and K^+/K couples in aqueous or PC solutions.[18] (C) Ionic conductivities of Li-, Na-, and K-based electrolytes with carbonate solvents.[19] (D) Desolvation energies of Li^+, Na^+, and K^+ in electrolytes containing EC or PC solvents.[19]

electrolytes and lower desolvation energy at the electrolyte/electrode interface (Figure 1C,D).[19]

Unlike Li, K metal is inert to nitrogen, allowing the use of nitrogen atmospheres in battery fabrication in place of costly argon. Furthermore, K does not alloy with aluminum (Al),[20] enabling the use of low-cost Al (~1.3 $ per pound) current collectors instead of copper (~4.2 $ per pound), which further reduces production costs.[9] Moreover, the low melting point of K metal (63.5 °C, compared to 97.8 °C for Na and 180.5 °C for Li) enables dendrite suppression via Joule heating without igniting inflammable organic solvents, mitigating thermal runaway risks.[21] Collectively, these advantages position PMBs as a scalable and economically viable solution for large-scale and sustainable energy storage, with the potential to enable more resilient clean energy infrastructures.

Despite the high energy density enabled by the use of K metal anodes, stabilizing K plating/stripping, the half-reaction occurring at the anode, remains a formidable challenge.[22,23] The pronounced reactivity of K metal readily induces the decomposition of electrolyte solvents and salts upon contact with its surface. This reactivity is further exacerbated during plating, particularly under high-voltage charging conditions,[24] where an excess of electrons renders the K surface even more reductive. The resulting decomposition products form a passivation layer known as the solid-electrolyte interphase (SEI), which typically consists of an inorganic-rich inner layer and an organic-rich outer layer.[25] The SEI is critical for preventing continued parasitic reactions between the K metal and the electrolyte, while still allowing K^+ migration across the interface.

However, due to the "host-less" nature of the K metal anode during plating—where K adatoms directly adsorb onto nucleation sites and integrate into crystalline growth[26]—substantial, often conceptualized "infinite", volume expansion occurs. Uneven nucleation and self-reinforcing growth also promote dendrite formation and impose severe local mechanical stress on the SEI, causing fracture and exposing fresh K surface.[26] The renewed surface accelerates electrolyte consumption, exacerbates nonuniform K^+ flux, and further amplifies dendrite growth.[27] Under practical conditions—high areal capacity, high current density, limited electrolyte supply, and extreme temperatures—these degradation pathways are intensified, leading to premature failure and severe safety risks. Consequently, controlling K deposition morphology, suppressing dendrite growth, and engineering robust SEI composition and structure are central scientific challenges for advancing PMB technology.[28]

2. STRATEGIES FOR STABILIZING POTASSIUM METAL ANODES

A broad spectrum of stabilization strategies for K metal anodes has been proposed, including electrolyte engineering,[29] additive regulation,[30] artificial SEI construction,[31] separator modification,[32] and solid-state or polymer electrolytes.[33,34] These approaches have been comprehensively summarized in existing reviews.[28,35−40] This article focuses exclusively on substrate design as a distinct yet underexplored strategy for

https://doi.org/10.1021/acsaem.5c02661
ACS Appl. Energy Mater. XXXX, XXX, XXX−XXX

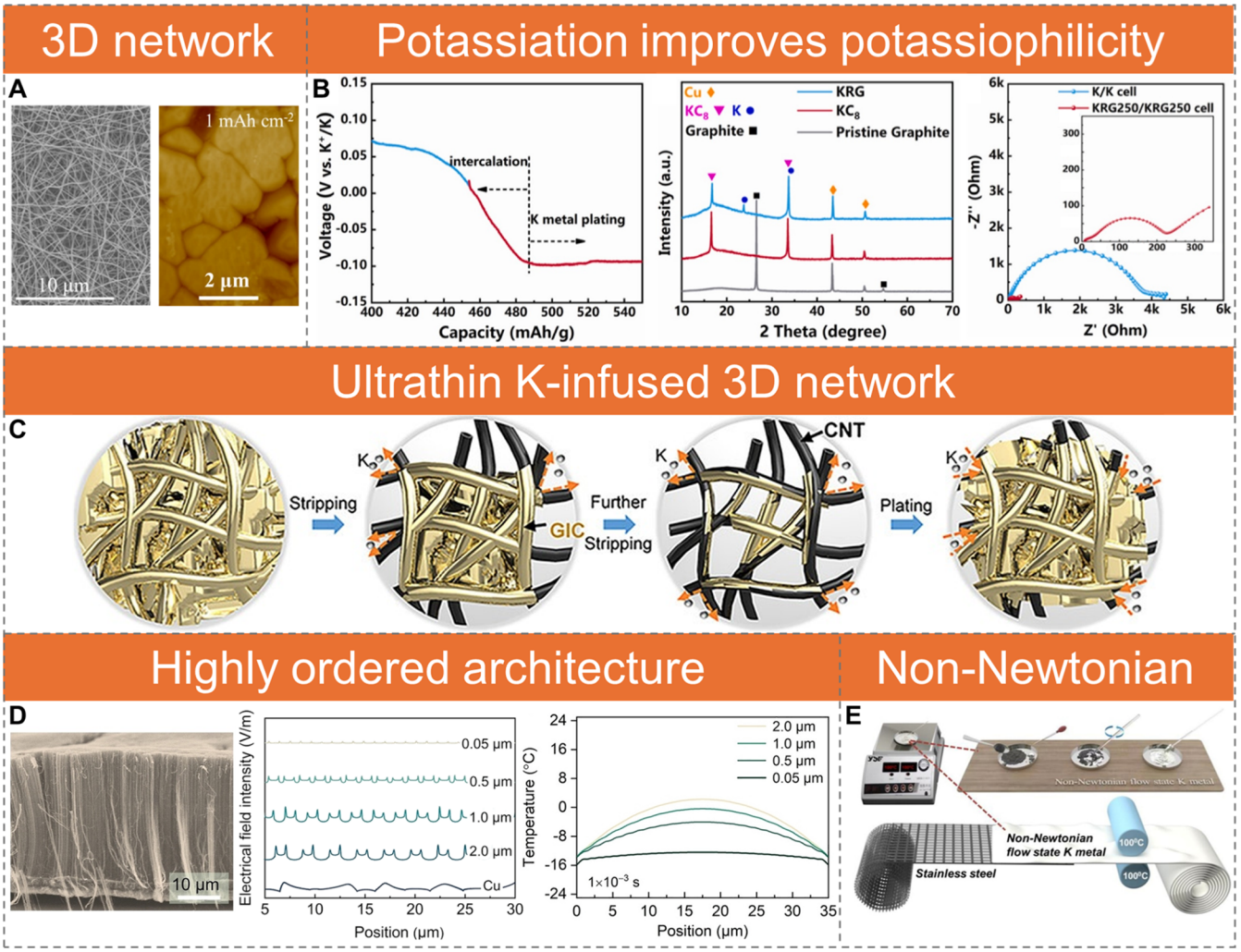

Figure 2. Structural engineering strategies for 3D host architectures. (A) SEM image of CNF and AFM image of K deposition (1 mAh cm^{-2}) on CNF. Reproduced with permission from ref 42. Copyright 2022 Elsevier. (B) Galvanostatic voltage profiles of K||graphite cells showing K intercalation and plating at a current density of 25 mA g^{-1}; XRD patterns of graphite anodes indicating the formation of KC_8 and K-rich graphite (KRG) during discharge; and Nyquist plots of K||K and KRG||KRG symmetric cells. Reproduced with permission from ref 44. Copyright 2023 Elsevier. (C) Schematic illustration of the K plating/stripping process within CNT networks. Reproduced from ref 45. Copyright 2024 American Chemical Society. (D) Cross-sectional SEM image of highly ordered CNTs, showing a dense film structure; electric field distribution plotted along the electrode, revealing high uniformity in regions with interspace gaps below 0.05 μm; temperature distribution of the thermal field at a highly ordered 1D nanoarray electrode with varying gap widths at 1×10^{-3} s. Reproduced with permission from ref 48. Copyright 2023 John Wiley and Sons. (E) Schematic of the synthesis process for non-Newtonian flow-state K metal using a stainless-steel substrate. Reproduced with permission from ref 50. Copyright 2023 Elsevier.

stabilizing K metal anodes. We synthesize recent advances in substrate-engineering approaches that regulate K nucleation, deposition morphology, and SEI formation. Five principal strategies are classified and compared: three-dimensional (3D) conductive hosts, heteroatom doping and molecular grafting, inorganic nanoparticle incorporation, alloying seeds, and work-function engineering. Each strategy is evaluated in terms of its underlying mechanism, demonstrated benefits, practical limitations, and remaining challenges.

2.1. Structural Engineering via Three-Dimensional Host Architectures. 3D conductive hosts are a primary strategy to mitigate the severe volume changes and dendritic growth of K metal. They (i) expand the effective nucleation area to reduce local current density, (ii) provide internal voids to accommodate deposited K, and (iii) undergo potassiation (e.g., KC_8 formation) that strengthens K−substrate binding and lowers interfacial impedance. Typically, a 3D host−K composite anode is fabricated via a two-step process: (i) synthesis of a porous, conductive substrate, often carbon-based networks or metallic foams; and (ii) infusion of K metal into the host voids. The morphology of initially deposited K nuclei largely dictates subsequent deposition behavior and, therefore, the cycling stability of the anode.

Applying a simple carbon paper (CP) layer on a K metal surface significantly reduces plating/stripping polarization and improves cycling stability, underscoring the ability of 3D carbon networks to regulate K deposition.[41] Infusing K metal into carbon nanofiber (CNF)[42] and carbon nanotube (CNT)[43] networks further lowers nucleation overpotential and promotes uniform deposition (Figure 2A). This improvement arises from the potassiation of highly graphitic carbon, forming KC_8 prior to plating, which decreases interfacial impedance compared to bare K metal foil (Figure 2B). This KC_8 phase increases the binding energy of K atoms from

https://doi.org/10.1021/acsaem.5c02661
ACS Appl. Energy Mater. XXXX, XXX, XXX−XXX

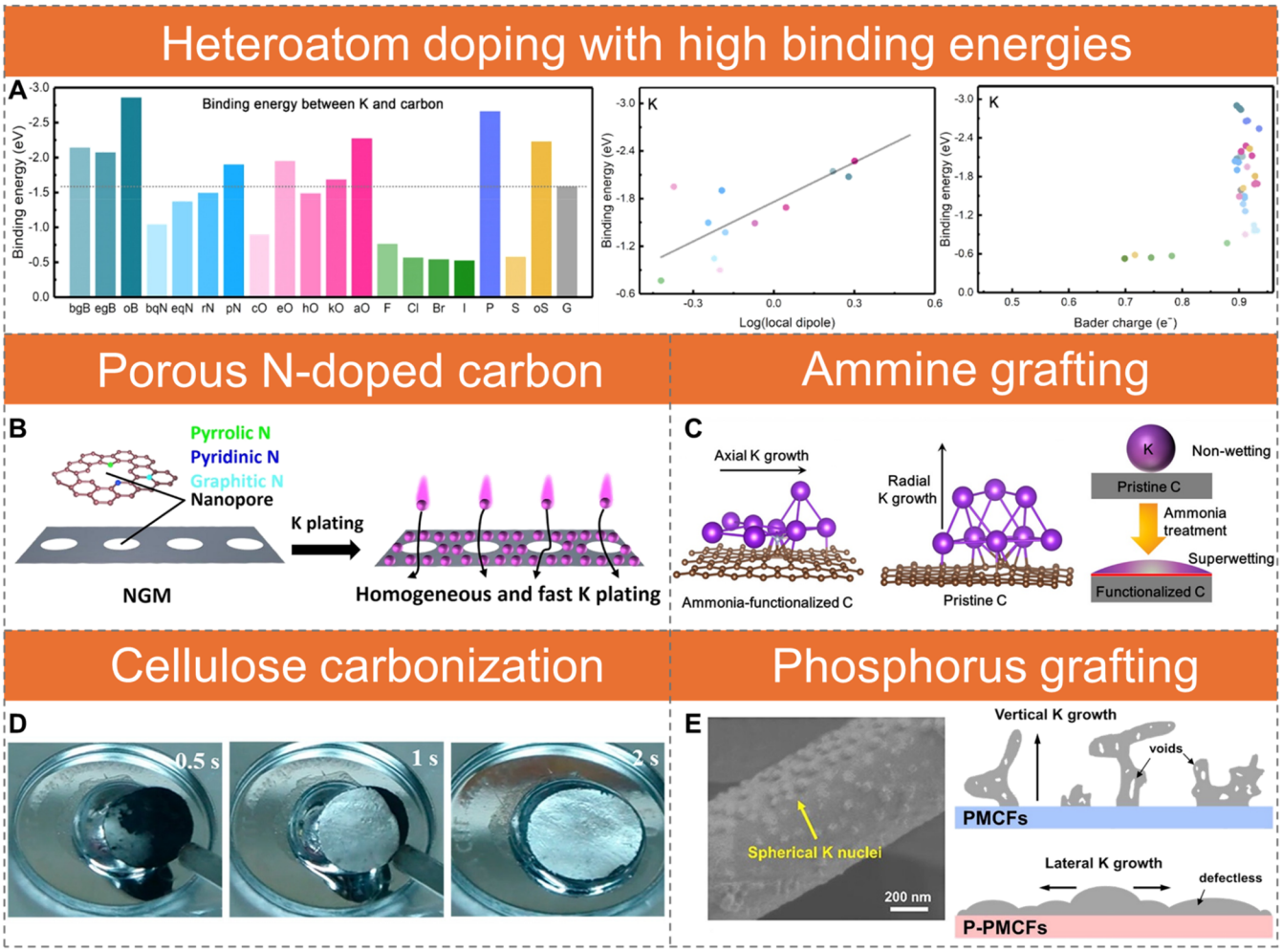

Figure 3. Heteroatom doping and molecular grafting strategies for electron localization. (A) Binding energy between K atoms and doped carbons, showing the correlation between K binding energy, log(local dipole), and charge transfer. Reproduced with permission from ref 51. Copyright 2020 Elsevier. (B) Schematic of a porous N-doped carbon that enables homogeneous and rapid K plating. Nanopores provide direct pathways for K ions to access the entire electrode. Reproduced with permission from ref 52. Copyright 2022 Elsevier. (C) DFT calculations of K growth on ammonia-treated and untreated carbon surfaces. Atom colors: C (gray), N (blue), H (white), K (purple). Inset: schematic illustration showing significantly improved wettability of K metal on the functionalized carbon host. Reproduced from ref 53. Copyright 2022 American Chemical Society. (D) Photographs showing molten K infusion into carbonized bacterial cellulose scaffolds, demonstrating high potassiophilicity. Reproduced from ref 54. Copyright 2021 American Chemical Society. (E) SEM images of K nucleation morphology on P-grafted porous CNFs after K plating at 1 mA cm^{-2} for 18 s, along with schematics of K growth behavior on porous CNFs and P-grafted porous CNFs. Reproduced from ref 62. Copyright 2024 American Chemical Society.

−0.78 eV for graphite (110) and −0.73 eV for K (110) to −1.55 eV for KC_8 (002), thereby enhancing the potassiophilicity of the carbon host.[44] This, combined with reduced local current density, contributes to the observed decrease in nucleation overpotential and impedance.

CNTs, with a high specific surface area of 92.2 m^2 g^{-1}, can increase the K binding energy up to −3.09 eV.[45] The strong interaction within the K@CNT composite significantly enhances its mechanical properties, increasing the Young's modulus from 1.4 GPa (K metal) to ∼8.8 GPa and elevating the effective melting point from 63.5 to ∼300 °C. This enables fabrication of flexible electrodes with tunable thicknesses ranging from ∼30 to ∼200 μm and corresponding areal capacities from ∼1.77 to ∼11.82 mAh cm^{-2}. The K@CNT composite anode enables uniform K plating/stripping along the conductive CNT network, effectively suppressing dendrite growth via in-plane ion regulation (Figure 2C). It supports high areal current densities up to 10 mA cm^{-2} with stable cycling in symmetric cells. In full cells with a Prussian white (PW) cathode (∼7.7 mg cm^{-2}), it delivers a reversible capacity of 65.8 mAh g^{-1} at 200 mA g^{-1}. A 12 mAh pouch cell further achieves 187.3 Wh kg^{-1} without prepotassiation, demonstrating the viability of K-infused CNTs as scalable alternatives to bare K metal anodes.

Aligned CNT architecture further enhances the electronic and ionic transport, improving redox kinetics and promoting stable cycling and capacity retention in PMBs.[46,47] Highly ordered one-dimensional (1D) CNT nanoarrays with sub-0.05 μm spacing ensure uniform electric and thermal field distributions (Figure 2D).[48] K deposition on these aligned CNTs results in large, smooth domains, in stark contrast to the irregular, whisker-like, or fractured deposits observed on graphene and Cu electrodes. Notably, highly ordered CNTs enable stable K plating/stripping at −20 °C for over 70 cycles, whereas Cu and graphene electrodes fail under the same conditions. Full cells using perylene-3,4,9,10-tetracarboxylic

https://doi.org/10.1021/acsaem.5c02661
ACS Appl. Energy Mater. XXXX, XXX, XXX−XXX

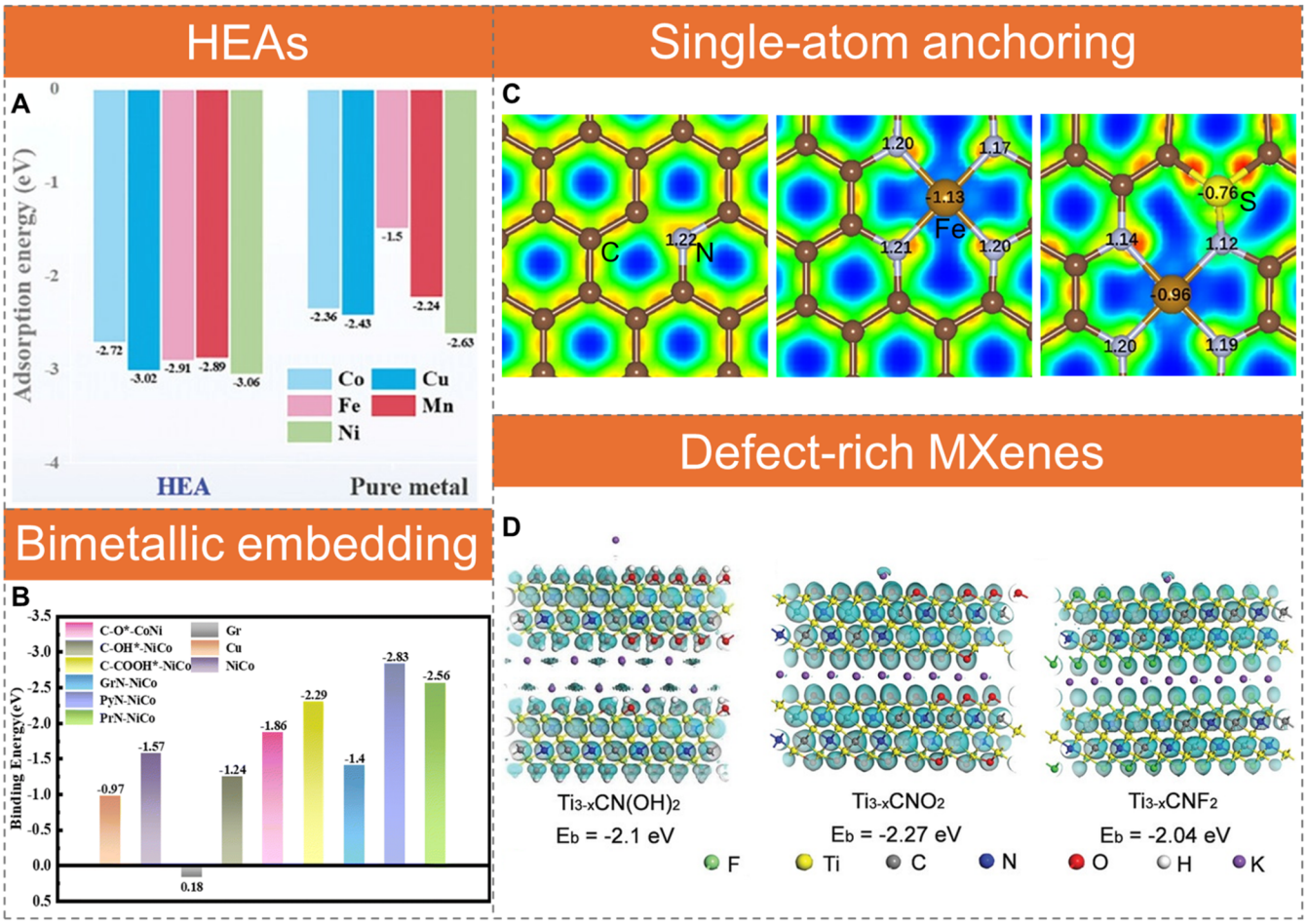

Figure 4. Inorganic incorporation for electron localization. (A) Adsorption energies of a K ion on Mn, Fe, Co, Cu, and Ni sites in HEA compared to their pure metal counterparts. Reproduced with permission from ref 70. Copyright 2024 John Wiley and Sons. (B) Binding energies of a K atom on Cu and on pristine and modified NiCo@N,O-doped graphene surfaces. Reproduced with permission from ref 72. Copyright 2023 Royal Society of Chemistry. (C) Electron localization function (ELF) maps of N-doped graphene, single-atom Fe@N-doped graphene, and single-atom Fe@N,S-doped graphene. Electron density increases from blue to green, yellow, and red. Reproduced with permission from ref 76. Copyright 2025 John Wiley and Sons. (D) Density functional theory (DFT)-calculated deformation charge density of K atoms adsorbed on $Ti_{3-x}CNO_2$, $Ti_{3-x}CN(OH)_2$, and $Ti_{3-x}CNF_2$. Reproduced with permission from ref 85. Copyright 2019 John Wiley and Sons.

dianhydride (PTCDA) cathodes retain over 80% of their room-temperature capacity at −20 °C, further demonstrating the low-temperature viability of this system. These findings underscore the critical role of electric field regulation for uniform deposition.[49]

Moreover, mixing K metal with carbon black (Super P) at 80 °C produces a non-Newtonian K@Super P composite exhibiting shear-thinning and thixotropic behavior, likely due to bond formation between K and Super P (Figure 2E). When coated onto stainless steel, this composite forms a self-supporting, flexible electrode that reduces localized stress and prevents cracking.[50]

3D hosts effectively reduce nucleation overpotential, suppress dendrite formation, and enable high areal capacity and improved mechanical resilience. However, many high-surface-area architectures compromise tap/volumetric density, increase electrolyte uptake, and introduce fabrication complexity, making lean-electrolyte operation difficult. Moreover, spatially resolved deposition pathways within complex pores remain insufficiently understood. Future work should (i) optimize pore structure and surface area to balance areal and volumetric energy density, (ii) establish scalable, low-cost synthesis of ordered 3D hosts, and (iii) integrate operando imaging with modeling to elucidate deposition dynamics under practical conditions such as high areal loading, lean electrolyte, and varied temperatures.

2.2. Electron Localization via Heteroatom Doping and Molecular Grafting. Heteroatom doping and molecular grafting modify local electronic structures and create dipolar or charged sites that significantly enhance K adsorption energy and wettability, thereby guiding nucleation and promoting uniform deposition. First-principles calculations on graphene nanoribbons doped with B, N, O, F, P, S, Cl, Br, and I reveal a wide range of binding energies for K atoms (Figure 3A).[51] Among these, F, Cl, Br, and I are identified as ineffective dopants, exhibiting lower K binding energies than pristine graphene. In contrast, effective dopants such as B−2C−O-type boron (oB) codoping exhibit the highest binding energy (−2.86 eV), followed by P-doping (−2.67 eV), carboxyl groups (aO), sulfonyl groups (oS), and pyridinic nitrogen (pN). These high binding energies are attributed to strong dipoles formed between the doping atoms and their adjacent atoms, as well as significant charge transfer (Bader charge)

https://doi.org/10.1021/acsaem.5c02661
ACS Appl. Energy Mater. XXXX, XXX, XXX−XXX

exceeding 0.89 electrons from K atoms to the doping sites (Figure 3A).

Experimental evidence supports these predictions. Pyridinic N doping reduces charge transfer resistance and polarization, while micro/nanoporous structures in N-doped carbon facilitates rapid K^+ transport, yielding a high K^+ diffusion coefficient (Figure 3B).[52] Similarly, NH_3-functionalized carbon cloth (CC) exhibits strong wettability toward molten K, guiding axial deposition and preventing dendritic growth, unlike pristine CC, which remains nonwetting and induces radical K growth (Figure 3C).[53] Carbonization of bacterial cellulose produces potassiophilic CNFs enriched with oxygen-containing functional groups, such as carboxyl and ketone groups, which exhibit strong K adsorption and high potassiophilicity with rapid molten K infusion (Figure 3D), thereby lowering the K nucleation overpotential.[54] Oxygen functionalities can also be introduced through reduced graphene oxide (rGO),[55−57] molecular oxygen grafting,[58] air heat treatment,[59] or annealing with oxygen-rich precursors.[60] Codoping with N, O, and S further enhances performance.[61] Additionally, porous CNFs grafted with red phosphorus via evaporation-deposition form P nanoclusters anchored by C−P bonds, creating abundant K nucleation sites.[62] This design promotes uniform in-plane deposition and suppresses perpendicular dendrite growth, resulting in 85% capacity retention after 1000 cycles at 20 C for perylene-3,4,9,10-tetracarboxylic dianhydride (PTCDA) cells (Figure 3E).

These approaches offer atomic-level tunability, compatibility with low-cost carbon scaffolds, and consistent reductions in nucleation barriers, leading to improved deposition uniformity. Their challenges include identifying the most effective dopant motifs (type, site, and coverage), mitigating the instability of grafted groups during cycling, and ensuring reproducibility at scale. Future research should integrate targeted DFT screening with standardized operando diagnostics to establish structure−function correlations, while prioritizing designs that preserve dopant functionality under repeated cycling and lean-electrolyte conditions.

2.3. Electron Localization via Inorganic Incorporation. Decorating hosts with inorganic nanoparticles or embedding active phases induces local electron redistribution and generates strong adsorption sites for K, thereby lowering nucleation overpotential and improving deposition morphology. Transition metals such as Ag,[63,64] Au,[65] and Pd,[66] as well as alloys like Cu_6Sn_5,[67] Cu_3Pt,[68] and GaInNi,[69] exhibit strong binding energies with K, effectively lowering nucleation overpotential and promoting uniform K deposition. High-entropy alloys (HEAs), composed of five or more metallic elements, generate surface regions with electron accumulation and depletion, thereby enhancing K^+ adsorption. For instance, equimolar MnFeCoCuNi HEA nanoparticles exhibit electron enrichment at Cu and Ni sites, enhancing K^+ binding beyond that of the corresponding elemental metals (Figure 4A).[70] This enables PTCDA cells to deliver a reversible capacity of 66 mAh g^{-1} (58% capacity retention) and nearly 100% Coulombic efficiency (CE) after 2000 cycles at 20 C.

Synergistic effects also arise when metals are embedded into heteroatom-doped carbon. For example, elemental Co alone binds weakly with K^+, but when embedded in N-doped carbon, it increases surface electron density of the carbon, enhancing K^+ adsorption and improving potassiophilicity.[71] Similar benefits are observed in bimetallic systems such as NiCo[72] and CoZn,[73] where NiCo embedded in N,O-doped carbon exhibits the strongest K atom adsorption at the pyridinic N configuration, surpassing both O-containing carbon@NiCo and bare NiCo (Figure 4B). Downsizing metals to quantum dots or single atoms further amplifies their effectiveness. Cu quantum dots,[74] single-atom Co,[75] and single-atom Fe[22] anchored on N-doped or N,S-doped carbon provide abundant nucleation sites and exhibit strong K adsorption, driven by enhanced electron localization at N sites induced by the metal nanoclusters or atoms.

Single-atom Fe, coordinated with N dopants ($Fe−N_4$), increases electron density at adjacent N sites, while additional S doping further strengthens electron localization (Figure 4C).[76] The integration of Fe nanoclusters with single-atom Fe promotes cooperative electron donation, shifting the d-band center closer to the Fermi level and thereby strengthening overall K binding.[77] Compounds with localized electrons can also show strong K binding; examples include $CoWO_4$ (electron localization via lattice distortion)[78,79] and α-phase MoC (significant Mo-to-C electron transfer).[80,81]

MXenes, a family of two-dimensional (2D) transition metal carbides, nitrides, and carbonitrides, form strong covalent metal (M)-C/N bonds and can promote uniform deposition.[82,83] Ti_3C_2 MXene nanoribbons, for instance, provide a 3D woven-like framework for uniform K plating.[84] Introducing Ti vacancies and surface terminations (−O, −OH, −F) in $Ti_{3-x}CNT_y$ structures further improves K binding energy and reduces nucleation overpotential from 33 mV to as low as 6 mV.[85] The surface groups modulate the electronic structure of adjacent C/N atoms,[86] yielding binding energies of −2.27 eV for $Ti_{3-x}CNO_2$, −2.10 eV for $Ti_{3-x}CN(OH)_2$, and −2.04 eV for $Ti_{3-x}CNF_2$ (Figure 4D).[85] Zeolitic imidazolate framework-8 (ZIF-8), a nitrogen-rich metal−organic framework (MOF), also enhances plating/stripping stability through its nanoporous structure, abundant surface functional groups, and nitrogen active sites.[87]

Inorganic additives provide strong and tunable K binding, reinforce host mechanics, and create synergistic effects, such as enhanced electron density and cooperative binding, when integrated with doped carbons. However, challenges include heterogeneous dispersion, potential electronic insulation if poorly integrated, unintended catalytic side reactions with electrolytes, high costs for certain metals, and scale-up difficulties. The long-term electrochemical stability of nanoparticle−electrolyte interfaces also requires rigorous evaluation. Future efforts should focus on engineering well-integrated, conductive inorganic−carbon interfaces with controlled spatial distribution, emphasizing earth-abundant elements, conductive encapsulation to avoid insulating shells, and systematic operando/accelerated aging studies.

2.4. Interfacial Reconstruction via Alloying Seeds. Alloying seeds provide a different approach: instead of passive adsorption, reactive seeds form K-containing alloys that act as thermodynamically favorable nucleation sites with near-zero interfacial energy, thereby reducing nucleation overpotential and enabling homogeneous deposition.[26] When dispersed within a 3D matrix, these alloying seeds undergo spontaneous alloying reactions, which are thermodynamically favorable, and subsequently promote site-specific deposition on the resulting alloy phases. To date, Bi-, Zn-, and Sn-based metals or their reactive compounds have been most widely explored.

Bi-based alloying seeds have been implemented via Bi nanoparticles,[88,89] direct surface coatings,[90] and reactive oxides such as Bi_2O_3.[91] For instance, Bi_{80} nanoclusters anchored on

https://doi.org/10.1021/acsaem.5c02661
ACS Appl. Energy Mater. XXXX, XXX, XXX−XXX

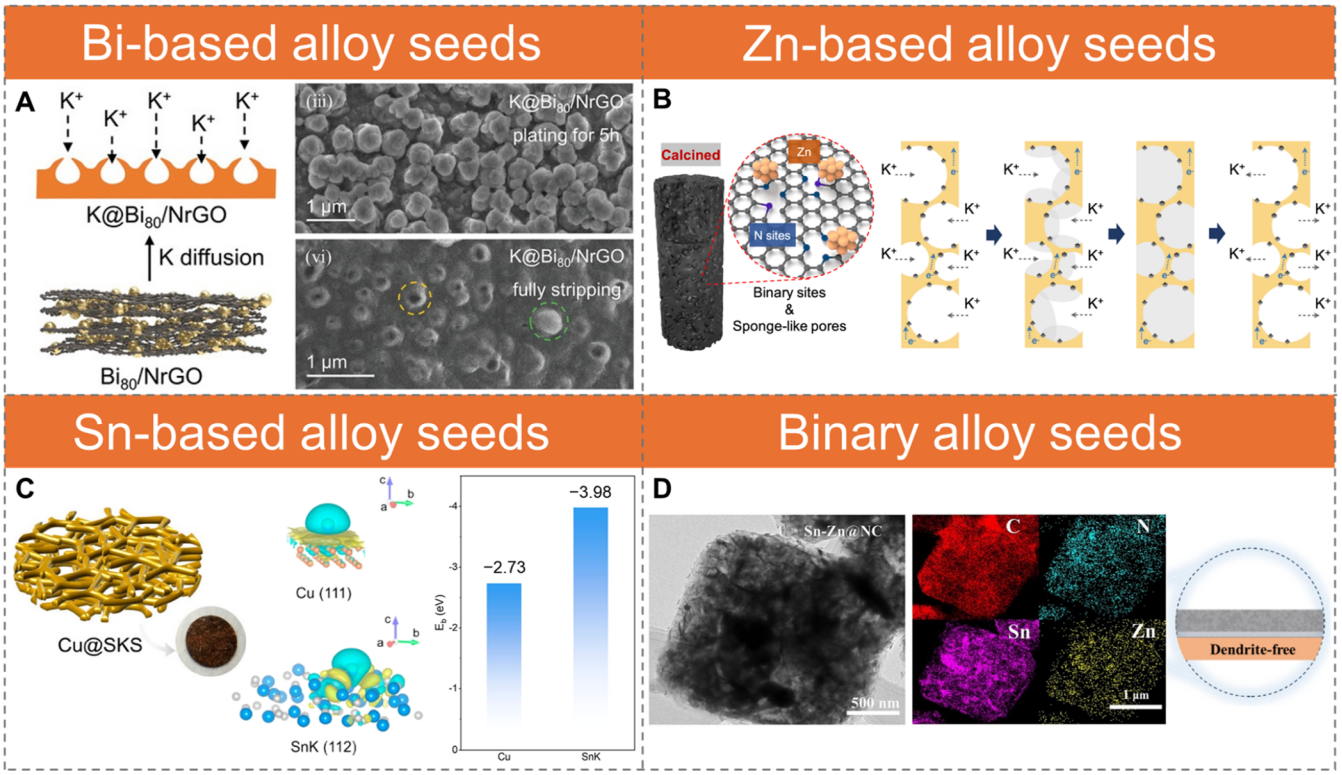

Figure 5. Alloying-seed strategies for interfacial reconstruction. (A) Schematic illustration of K plating on a K@Bi_{80} anchored on N-doped rGO. SEM images show the evolution of K morphology during plating/stripping. During plating, the hollow pores of K@Bi_{80} gradually fill with K metal, forming small, brighter spheres. After stripping, the hollow pore structure reappears with lower contrast (yellow dashed circles), indicating structural preservation and residual unstripped K. Reproduced with permission from ref 92. Copyright 2023 John Wiley and Sons. (B) Schematic of N-doped porous CNFs anchored with Zn clusters and the corresponding K plating/stripping process. Reproduced from ref 99. Available under a CC-BY 4.0 license. Copyright 2022 Siwu Li et al. (C) Schematic and optical image of the SnK alloy@Cu substrate. Differential charge density plots at K^+ adsorption sites on Cu(111) and SnK(112) surfaces. Yellow and light blue indicate charge accumulation and depletion, respectively (isosurface level: 0.0002 e $Bohr^{-3}$). Blue, gray, and orange spheres represent K, Sn, and Cu atoms. Binding energies of Cu and SnK alloy are also shown. Reproduced from ref 105. Copyright 2023 American Chemical Society. (D) TEM image of binary Sn−Zn@N-doped carbon and corresponding elemental mappings of C, N, Sn, and Zn. Schematic illustration of uniform K deposition. Reproduced with permission from ref 106. Copyright 2025 Elsevier.

N-doped rGO develop dense hollow pores after molten K infusion (Figure 5A).[92] The dynamic alloying-dealloying process enables reversible pore restoration during cycling, directing K to deposit within the pores, suppressing dendrites, and lowering the nucleation overpotential to ∼5 mV. The PW cells achieve a capacity of ∼65 mAh g^{-1} with negligible degradation and ∼99% CE at 1000 mA g^{-1} after 1960 cycles.

Zn-based alloying seeds, including metallic Zn[93] and compounds such as ZnO,[94−96] ZnF_2,[97] and ZnTe,[98] react with K to form Zn−K alloys during plating. Zn nanoclusters embedded in porous N-doped CNFs generate dual active sites: Zn functions as the alloying center, while N dopants provide strong K binding (Figure 5B).[99] The uniform distribution of these binary seeds within high-surface-area nanopores promotes homogeneous K nucleation and deposition, thereby enhancing deposition uniformity and improving host volume utilization (Figure 5B).

Sn-based alloying seeds, derived from elemental Sn,[100] SnO_2,[101−103] SnS_2,[104] or $SnBr_2$,[25] also show strong potassiophilicity. Sn-coated Cu foam, after prepotassiation, forms SnK alloys with a high K binding energy (−3.98 eV for SnK (211) versus −2.73 eV for Cu(111)), enabling stable plating/stripping (Figure 5C).[105]

Binary alloying seeds are further investigated. Comparative studies indicate that binary Sn−Zn outperforms binary Bi−Zn in cycling stability, likely due to lower K^+ diffusion barriers in KSn_2 (Figure 5D).[106] Other alloying elements such as Sb,[107] Sb_2O_3,[108] GeO_2,[109] and Hg[110] have also proved effective in extending PMB cycling life. In addition to alloy seeds, certain reactive but nonalloy-forming compounds—such as partially selenized copper oxyselenide (Cu−OSe) nanowires,[111] CuSe coatings,[112] MoS_2 microparticles,[113] CuO nanoparticles,[114] nanomesh porous NiO,[115] NiO nanoparticles,[116] and S layers[117]—have demonstrated improvements in cycle stability by modifying deposition pathways and suppressing dendrite growth.

Alloy seeds achieve extremely low nucleation barriers and dynamically reconstruct interfaces to confine deposition within engineered pores, yielding excellent morphological control and stable cycling. Their limitations include side reactions, partial irreversibility of alloying−dealloying, volume fluctuations in alloy phases, and possible dependence on costly or toxic elements, all of which challenge long-term stability and scalability. Future directions include (i) designing alloy compositions that balance potassiophilicity, reversibility, and cost, (ii) developing confinement strategies to prevent seed agglomeration or pulverization, and (iii) conducting mechanistic studies to quantify alloying kinetics and their interplay with SEI evolution under practical cycling conditions.

https://doi.org/10.1021/acsaem.5c02661
ACS Appl. Energy Mater. XXXX, XXX, XXX−XXX

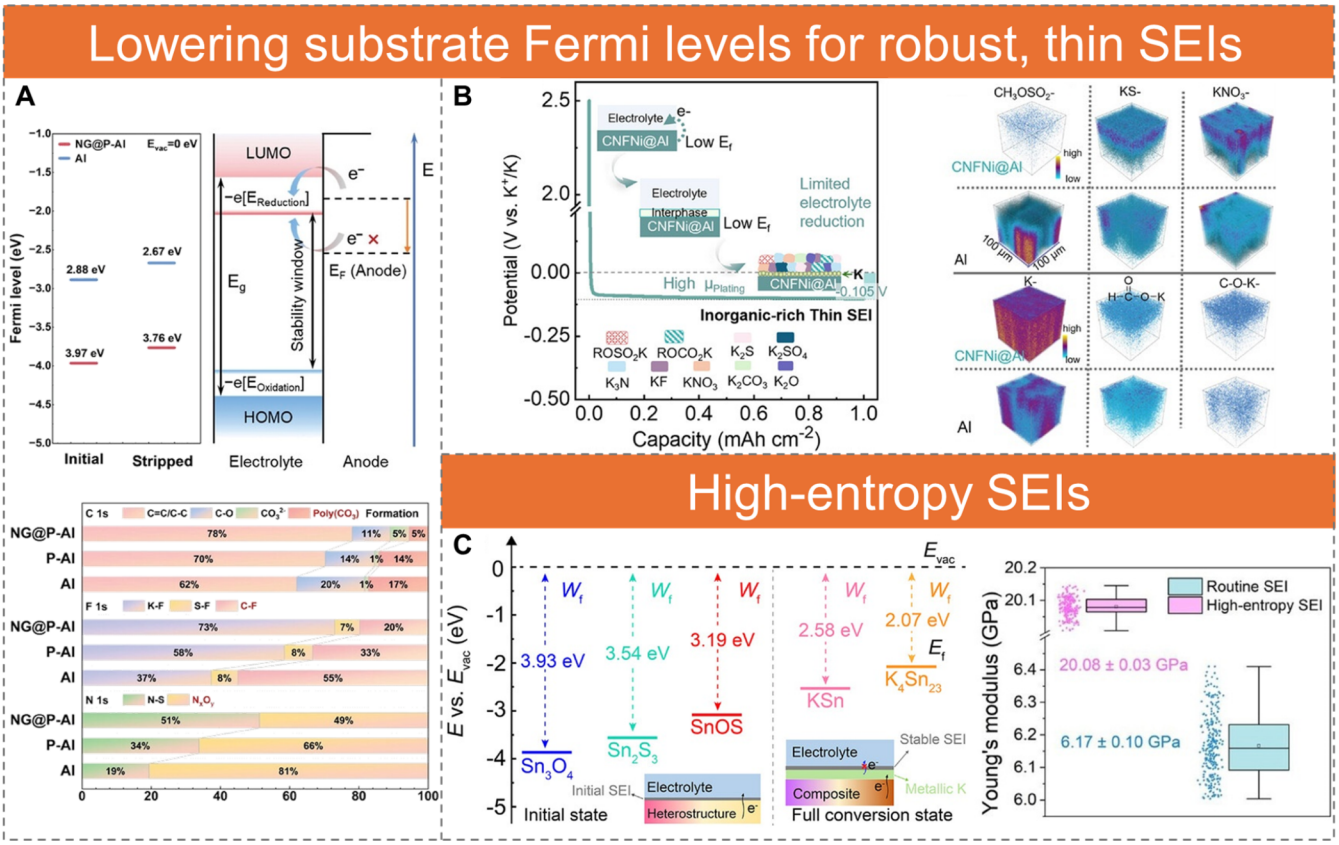

Figure 6. Substrate work function modulation for SEI engineering. (A) Fermi levels of NG@P−Al and Al at the initial and stripped stages, determined by extrapolating the secondary cutoff region in the UPS profiles. Schematic of SEI formation at the anode interface, and SEI chemical configurations with corresponding content percentages for all current collectors at the formation stage. Reproduced with permission from ref 119. Copyright 2023 John Wiley and Sons. (B) Schematic of SEI formation on CNFNi@Al current collectors during the first K plating in a three-electrode system without a formation period. TOF-SIMS 3D renderings of CH_3OSO_2, KS, KNO_3, K, HCO_2K, and C−O−K signals. Reproduced with permission from ref 120. Copyright 2025 John Wiley and Sons. (C) Calculated work functions of Sn_3O_4, Sn_2S_3, SnOS heterostructure, KSn, and K_4Sn_{23}, along with statistical values of Young's modulus. Reproduced with permission from ref 122. Copyright 2025 John Wiley and Sons.

2.5. SEI Engineering via Substrate Work Function. The substrate not only governs the morphology of K deposition but also shapes the composition and structure of the SEI. One straightforward approach involves pretreating substrates with SEI-forming compounds (e.g., NaF) to promote robust, inorganic-rich interphases.[118] Substrate electronic properties, particularly its Fermi level (E_f) and work function ($\Phi = E_{vac} - E_f$, where E_{vac} = 0 eV), directly affect interfacial electron flux during early plating, thereby determining electrolyte decomposition pathways and the organic/inorganic balance of the SEI.

A higher work function (lower E_f) decreases electron transfer to electrolyte molecules, suppressing the decomposition of neutral solvents while allowing preferential anion decomposition, thereby producing inorganic-rich SEIs. For example, direct growth of N-doped graphene on porous Al (NG@P−Al) via plasma-enhanced chemical vapor deposition raises the work function from 2.88 eV (bare Al) to 3.97 eV (Figure 6A), as measured by ultraviolet photoelectron spectroscopy (UPS).[119] After K plating and stripping, NG@P−Al retains a high work function of 3.76 eV, compared with 2.67 eV for bare Al. The resulting SEI contains the lowest fraction of organic species of poly(CO_3), C−F, and N_xO_y species, and the highest KF content, indicating a high inorganic-to-organic ratio and enhanced salt-derived composition.

Similar effects are achieved by directly spraying nickel (Ni)-embedded carbon nanofibers (CNFNi@Al) onto Al current collectors.[120] The embedded Ni species (Ni, NiO, Ni_3N, and Ni_3C) and carbon framework increase the work function to 4.2 eV, attributed to the higher electronegativity of Ni and CNF compared with Al, which reduces electron density at the surface and limits solvent decomposition (Figure 6B). This promotes the formation of a thin SEI and lowers electron tunneling probability, as the decreased E_f suppresses electron tunneling in quantum mechanical terms. CNFNi@Al also lowers nucleation overpotential and raises the plating plateau to −0.105 from −0.152 V for Al, which intensifies electrolyte decomposition and yields an organic-rich SEI. Time-of-flight secondary ion mass spectrometry (TOF-SIMS) confirms that CNFNi@Al produces a thin, uniform SEI enriched in anion-derived species (KS^-, KNO_3^-) with minimal solvent decomposition products ($CH_3OSO_2^-$), whereas bare Al exhibits deeper solvent degradation, producing HCO_2K-dominated layers throughout the SEI (Figure 6B). Under a low N/P ratio of 1, the PW cells deliver ∼105 mAh g^{-1} at 100 mA g^{-1} for 100 cycles. The low-Fermi-level current collector strategy has also proven effective in LMBs.[121]

Borrowing from the concept of high-entropy materials, a "high-entropy SEI" strategy has been proposed, incorporating five or more inorganic components to generate abundant grain boundaries that facilitate K^+ transport and reduce concen-

https://doi.org/10.1021/acsaem.5c02661
ACS Appl. Energy Mater. XXXX, XXX, XXX−XXX

tration gradients.[122] For example, hydrothermally coating 3D nickel foam with a Sn_3O_4/Sn_2S_3 heterostructure (SnOS@NF) induces complex electrochemical reactions that yield K_2SO_3, K_2CO_3, K_2S, K_2O, and KF during cycling. After complete conversion during K plating, the heterostructure transforms into KSn and K_4Sn_{23} alloys with low work function values of 2.58 and 2.07 eV, respectively, significantly lower than those of Sn_3O_4, Sn_2S_3, or the SnOS heterostructure (Figure 6C). This leads to further electrolyte decomposition to enrich the SEI components. The diversified components produce a high-modulus SEI (average ~ 20 GPa) compared with conventional SEIs (~6 GPa), thereby enhancing mechanical integrity. This allows the PW cells to retain 82.9 mAh g^{-1} after 1050 cycles at 2C.

Looking forward, integrating substrate engineering with controlled sacrificial chemistries offers a promising pathway: (i) tailoring or grading substrate work functions to homogenize electron flux, and (ii) seeding multicomponent inorganic SEIs for enhanced stability. Future efforts should focus on mapping work function (Kelvin probe force microscopy,[123] scanning tunneling spectroscopy[124]) and SEI composition (TOF-SIMS), quantifying SEI entropy and mechanics, and leveraging data-driven screening of precursor combinations. Scalable fabrication methods such as spray coating, plasma-enhanced chemical vapor deposition (PECVD), or atomic layer deposition (ALD) will be key for practical translation, with attention to compatibility under lean electrolyte and high areal capacity conditions. Key risks to manage are interfacial impedance from overly insulating layers and unintended catalytic routes from embedded metals.

3. CONCLUSIONS AND OUTLOOKS

Stabilizing K metal anodes requires a multifaceted strategy that integrates structural, chemical, and electronic design principles. Progress in understanding K deposition behavior and SEI formation, combined with scalable and cost-effective fabrication methods, is essential for advancing PMBs as sustainable, high-performance energy storage technologies. Substrate design provides promising pathways, and Table 1 summarizes the advantages and limitations of current strategies, highlighting mechanistic insights and unresolved challenges.

From a commercialization perspective, scalability and cost remain decisive. 3D carbon-based hosts, heteroatom-doped carbons, and carbons incorporated with inorganic components deliver strong performance at relatively low cost, particularly when derived from biomass or inexpensive precursors. Alloying-seed strategies are highly effective in controlling deposition but often rely on costly elements. Substrate work function engineering offers a scalable, manufacturing-compatible route, while high-entropy SEI designs show potential for long-term stability but require careful precursor selection.

Although significant progress has been made, the next decisive step is translating proof-of-concept advances into scalable and manufacturable technologies. This transition can be accelerated by the following priorities, supported by targeted experimental efforts.

3.1. K Deposition Pathways in 3D Hosts. 3D hosts are among the most promising strategies for stabilizing K metal anodes, yet the spatial pathways of K deposition within these architectures remain poorly resolved. K can deposit preferentially at the top surface, within the bulk, or at the bottom of the host, and the dominant pathway critically determines host volume utilization, mechanical stability, and interfacial

Table 1. Comparison of Various Substrate Design Strategies on Their Primary Mechanisms, Advantages, Challenges, Material Cost, Synthesis Complexity, and Near-Term Scalability[a]

strategy	representative materials	primary mechanisms	advantages	challenges	material cost (1–5)	synthesis complexity (1–5)	near-term scalability (1–5)
3D architectures	Carbon foams, CNT/CNF networks, MXene aerogels, metal foams	Lower local current density; buffer volume changes; guide uniform nucleation	Compatible with roll-to-roll; strong mechanical tolerance; dendrite suppression	Dead K accumulation if pores not wetted; molten K infusion often required	2–4	3–4	3
Doping and grafting	N, O, S (co)doped carbons; P and NH_3 grafted carbons	Enhance binding energy via electron localization; provide nucleation sites	Reduce nucleation overpotential; uniform K deposition	Rely on 3D carbon hosts; doping level control and reproducibility remain issues	1–2	2–3	4
Inorganic incorporation	Transition metals, alloys, carbides, oxides, nitrides, single-atom, MXenes	Enhance binding energy via electron localization; provide nucleation sites; inorganic-rich SEI	Reduce nucleation overpotential; strong chemical anchoring	Rely on 3D hosts; interfacial stability concerns and brittleness; complex synthesis for some materials	3–5	3–4	2–3
Alloying seeds	Bi, Zn, Sn, Sb, and Ge thin layers or particles	Transient K-M alloying lowers K nucleation barrier; abundant nucleation sites	Low nucleation overpotential; selective K plating	Use 3D hosts to improve efficiency; large volume fluctuations of alloying and dealloying	3–4	3–5	2
Substrate work function	N-doped graphene layers, Ni-embedded CNFs; Sn_3O_4/Sn_2S_3 heterostructures	Work function control preforms inorganic-rich, thin, ion-conductive, and robust SEIs	Lower continuous SEI repair, improved CE; manufacturing-friendly	Adhesion and thickness control are critical; work function control worths further study	2–3	3	4

[a]Semi-quantitative evaluation scores 1–5 from low to high.

https://doi.org/10.1021/acsaem.5c02661
ACS Appl. Energy Mater. XXXX, XXX, XXX−XXX

uniformity. To optimize host architectures, it is essential to establish how structural parameters (pore size, tortuosity, and conductivity gradients), chemical functionalities (heteroatom doping and inorganic incorporation), and electronic properties influence deposition pathways. These mechanistic insights will guide the rational design of 3D hosts with high K utilization, minimal dead volume, and long-term stability.

3.2. Substrate−Electrolyte Synergy. Substrate design cannot be optimized in isolation from electrolyte development. Electrolytes dictate interfacial reactions, SEI composition, and ionic transport, and their properties can either reinforce or offset the advantages of advanced substrates. For example, fluorinated solvents[125] and weak-solvation electrolytes[126] often yield inorganic-rich SEIs that synergize with substrates engineered for strong potassiophilicity, while functional additives[127] help stabilize interfaces during repeated plating and stripping.

The SEI on alkali-metal anodes is a dynamic, multilayered, and spatially heterogeneous film whose nanoscale morphology and chemistry evolve during cycling and with changes in electrolyte solvation.[128,129] Cryo-TEM and correlative chemical imaging have directly visualized nanoscale stratification, trapped metallic inclusions, and the nucleation of "dead" metal, correlating these features with local overpotential buildup and macroscopic electrochemical degradation.[130]

Inorganic fluorides such as LiF preferentially accumulate in the inner, inorganic-rich SEI sublayer during cycling.[131] While an LiF-rich layer enhances mechanical robustness, it may also hinder Li^+ transport under certain conditions, leading to ion-transport limitations.[132,133] Compared with Li, Na and K generally form more fragile and dynamically reconstructed SEIs and suffer greater initial losses of active metal inventory.[134] Consequently, reducing the intrinsic reactivity of solvent and salt components[135] represents a key design principle for improving interfacial stability in these systems.

Future progress will depend on codesign strategies that integrate substrate architecture and electrolyte formulation to establish robust, self-adaptive SEIs. Such synergistic approaches are likely to offer the most promising pathway toward durable, high-performance PMBs.

3.3. Integrated Data-Driven Modeling and Mechanistic Characterization. Couple atomistic, mesoscale, and continuum models with experimental data to build predictive frameworks for dendrite formation,[136] interfacial evolution,[137] and long-term cycling.[138] Multiscale modeling that couples DFT with phase-field simulations and continuum-scale models will be essential to capture K nucleation kinetics, ion transport, and stress evolution within complex 3D architectures. Employ machine learning for electrolyte and interface screening with uncertainty quantification to guide experimental design.[139]

Standardized post-mortem analyses of both electrodes should be performed to link degradation to performance decay. Key techniques include time-resolved operando microscopy and spectroscopy,[140] cryo-TEM for intact interface imaging,[141] operando XPS[142] and ToF-SIMS[143] for surface chemistry, neutron scattering[144] and solid-state NMR[145] for bulk and buried phases, and coupled gas analysis[146] with impedance monitoring to reveal failure pathways.[147]

3.4. Integration with Full-Cell Configurations and Scale-Up. Advance to full cells pairing high-performance cathodes with optimized electrolytes and realistic negative-to-positive capacity (N/P) ratios. Validate performance in long-format pouch cells under lean electrolyte and limited K excess, reporting cycle life at practical areal loadings, energy density, Coulombic efficiency,[148] impedance growth, gas generation,[146] and safety metrics.[149,150] Reports should consistently include parameters such as N/P ratios, electrolyte volume per areal capacity, stack pressure, and test temperature to enable cross-study comparison.[151,152]

3.5. Manufacturing and Sustainability. Transitioning from laboratory prototypes to industrially viable substrates requires scalable and cost-effective fabrication. Roll-to-roll coating, spray deposition, electrospinning, and chemical vapor deposition are promising techniques, but their compatibility with high-loading electrodes and uniform large-area coverage remains a bottleneck. Focus on processes compatible with roll-to-roll coating, dry-room operation, and cost-effective precursors. Incorporate cost models,[153] supply chain assessments,[154] solvent recovery,[155] and life-cycle analysis,[156] while developing strategies for recycling cathodes, K salts, separators, and current collectors.

3.6. Cross-Chemistry Transferability and Community Standards. Adapt insights from Li and Na systems while accounting for K-specific features such as ionic radius, solvation behavior, and SEI chemistry. Establish community-wide protocols, open data sets compliant with FAIR principles (Findable, Accessible, Interoperable, and Reusable),[157] and unified reporting metrics.[158] Publishing negative or marginal results should be encouraged to reduce redundant effort.

Accelerating the deployment of K metal anodes requires coordinated advances in mechanistic insights, multiscale modeling, realistic experimental designs, full-cell validation, sustainable manufacturing, and community-wide standards. Addressing the priorities outlined above will enable the transition from promising concepts to robust, cost-competitive, and scalable technologies.

While this review primarily focuses on K metal anodes, the underlying principles of substrate design show notable parallels with Li and Na counterparts. In all three systems, effective hosts mitigate dendritic growth by lowering local current density, improving metal−substrate binding, and directing uniform nucleation, while interfacial engineering strategies regulate SEI composition and mechanics. However, key distinctions arise from intrinsic material properties. K, with its larger ionic radius and weaker Lewis acidity, requires substrates with stronger potassiophilicity than those sufficient for Li or Na, and exhibits more pronounced volume fluctuations during deposition. Li metal benefits from relatively mature alloying and SEI-stabilization concepts, whereas Na and K highlight unique challenges in reversible alloying and SEI robustness under lean-electrolyte conditions. These differences underscore the need for tailored substrate chemistries rather than direct transference of Li-based designs.

AUTHOR INFORMATION

Corresponding Author

Yang Xu − *Department of Chemistry, University College London, London WC1H 0AJ, U.K.*; orcid.org/0000-0003-0177-6348; Email: y.xu.1@ucl.ac.uk

Author

Yupei Han − *Department of Chemistry, University College London, London WC1H 0AJ, U.K.*

Complete contact information is available at: https://pubs.acs.org/10.1021/acsaem.5c02661

https://doi.org/10.1021/acsaem.5c02661
ACS Appl. Energy Mater. XXXX, XXX, XXX−XXX

Notes

The authors declare no competing financial interest.

■ ACKNOWLEDGMENTS

Y.X. acknowledges the support from the Engineering and Physical Sciences Research Council (EP/X000087/1), Leverhulme Trust (RPG-2025−127), and Royal Society (IEC \NSFC\223016). Y.H. acknowledges the support from the China Scholarship Council (CSC).

■ REFERENCES

(1) Wang, F.; Harindintwali, J. D.; Yuan, Z.; Wang, M.; Wang, F.; Li, S.; Yin, Z.; Huang, L.; Fu, Y.; Li, L.; Chang, S. X.; Zhang, L.; Rinklebe, J.; Yuan, Z.; Zhu, Q.; Xiang, L.; Tsang, D. C. W.; Xu, L.; Jiang, X.; Liu, J.; Wei, N.; Kästner, M.; Zou, Y.; Ok, Y. S.; Shen, J.; Peng, D.; Zhang, W.; Barceló, D.; Zhou, Y.; Bai, Z.; Li, B.; Zhang, B.; Wei, K.; Cao, H.; Tan, Z.; Zhao, L.; He, X.; Zheng, J.; Bolan, N.; Liu, X.; Huang, C.; Dietmann, S.; Luo, M.; Sun, N.; Gong, J.; Gong, Y.; Brahushi, F.; Zhang, T.; Xiao, C.; Li, X.; Chen, W.; Jiao, N.; Lehmann, J.; Zhu, Y.-G.; Jin, H.; Schäffer, A.; Tiedje, J. M.; Chen, J. M. Technologies and Perspectives for Achieving Carbon Neutrality. *Innovation* **2021**, *2* (4), No. 100180.

(2) Liu, Z.; Deng, Z.; He, G.; Wang, H.; Zhang, X.; Lin, J.; Qi, Y.; Liang, X. Challenges and Opportunities for Carbon Neutrality in China. *Nat. Rev. Earth Environ.* **2022**, *3* (2), 141−155.

(3) Wu, F.; Maier, J.; Yu, Y. Guidelines and Trends for Next-Generation Rechargeable Lithium and Lithium-Ion Batteries. *Chem. Soc. Rev.* **2020**, *49* (5), 1569−1614.

(4) Zhang, S.; Li, R.; Deng, T.; Ma, Q.; Hong, X.; Zhang, H.; Zhang, R.; Ding, S.; Wu, Y.; Zhu, H.; Li, M.; Zhang, H.; Lu, D.; Ma, B.; Lv, L.; Li, Y.; Chen, L.; Shen, Y.; Guo, R.; Fan, X. Oscillatory Solvation Chemistry for a 500 Wh kg^{-1} Li-Metal Pouch Cell. *Nat. Energy* **2024**, *9* (10), 1285−1296.

(5) Huang, H.; Hu, Y.; Hou, Y.; Wang, X.; Dong, Q.; Zhao, Z.; Ji, M.; Zhang, W.; Li, J.; Xie, J.; Guo, H.; Han, X.; Ouyang, X.; Hu, W. Delocalized Electrolyte Design Enables 600 Wh kg^{-1} Lithium Metal Pouch Cells. *Nature* **2025**, *644*, 660−667.

(6) Jie, Y.; Wang, S.; Weng, S.; Liu, Y.; Yang, M.; Tang, C.; Li, X.; Zhang, Z.; Zhang, Y.; Chen, Y.; Huang, F.; Xu, Y.; Li, W.; Guo, Y.; He, Z.; Ren, X.; Lu, Y.; Yang, K.; Cao, S.; Lin, H.; Cao, R.; Yan, P.; Cheng, T.; Wang, X.; Jiao, S.; Xu, D. Towards Long-Life 500 Wh kg^{-1} Lithium Metal Pouch Cells via Compact Ion-Pair Aggregate Electrolytes. *Nat. Energy* **2024**, *9* (8), 987−998.

(7) Rudnick, R. L.; Gao, S. Composition of the Continental Crust. In *Treatise on Geochemistry*; Elsevier, 2014; pp 1−51 DOI: 10.1016/B978-0-08-095975-7.00301-6.

(8) Yin, J. Z.; Shi, A.; Yin, H.; Li, K.; Chao, Y. Global Lithium Product Applications, Mineral Resources, Markets and Related Issues. *Nat. Sci.* **2024**, *1*, 197−217.

(9) *Mineral Commodity Summaries*, 2025; https://pubs.usgs.gov/publication/mcs2025.

(10) Tabelin, C. B.; Dallas, J.; Casanova, S.; Pelech, T.; Bournival, G.; Saydam, S.; Canbulat, I. Towards a Low-Carbon Society: A Review of Lithium Resource Availability, Challenges and Innovations in Mining, Extraction and Recycling, and Future Perspectives. *Miner. Eng.* **2021**, *163*, No. 106743.

(11) Ma, X.; Zhang, D.; Fu, H.; Rao, A. M.; Zhou, J.; Fan, L.; Lu, B. Energy Band-Engineered Solid Electrolyte Interphase for Stable Potassium-Ion Batteries. *Joule* **2025**, *9*, No. 101952.

(12) Xu, Y.; Du, Y.; Chen, H.; Chen, J.; Ding, T.; Sun, D.; Ha Kim, D.; Lin, Z.; Zhou, X. Recent Advances in Rational Design for High-Performance Potassium-Ion Batteries. *Chem. Soc. Rev.* **2024**, *53* (13), 7202−7298.

(13) Xue, Y.; Chen, Y.; Liang, Y.; Shi, L.; Ma, R.; Qiu, X.; Li, Y.; Guo, N.; Zhuang, Q.; Xi, B.; Ju, Z.; Xiong, S. Substitution Index-Prediction Rules for Low-Potential Plateau of Hard Carbon Anodes in Sodium-Ion Batteries. *Adv. Mater.* **2025**, *37* (28), No. 2417886.

(14) Chen, Y.; Xi, B.; Huang, M.; Shi, L.; Huang, S.; Guo, N.; Li, D.; Ju, Z.; Xiong, S. Defect-Selectivity and "Order-in-Disorder" Engineering in Carbon for Durable and Fast Potassium Storage. *Adv. Mater.* **2022**, *34* (7), No. 2108621.

(15) Yang, R.; Qiu, X.; Xiong, H.; Cui, Z.; Xue, Y.; Zhou, R.; Jiang, J.; Kong, X.; Dong, L.; Zhuang, Q.; Ju, Z.; Chen, Y. Growth Space Engineering of Closed Pores in Hard Carbon for Low-Temperature Sodium-Ion Batteries. *Energy Storage Mater.* **2025**, *80*, No. 104415.

(16) Ma, M.; Chong, S.; Yao, K.; Liu, H. K.; Dou, S. X.; Huang, W. Advanced Anode Materials for Potassium Batteries: Sorting out Opportunities and Challenges by Potassium Storage Mechanisms. *Matter* **2023**, *6* (10), 3220−3273.

(17) Ding, H.; Wang, J.; Zhou, J.; Wang, C.; Lu, B. Building Electrode Skins for Ultra-Stable Potassium Metal Batteries. *Nat. Commun.* **2023**, *14* (1), No. 2305.

(18) Komaba, S.; Hasegawa, T.; Dahbi, M.; Kubota, K. Potassium Intercalation into Graphite to Realize High-Voltage/High-Power Potassium-Ion Batteries and Potassium-Ion Capacitors. *Electrochem. Commun.* **2015**, *60*, 172−175.

(19) Liu, P.; Mitlin, D. Emerging Potassium Metal Anodes: Perspectives on Control of the Electrochemical Interfaces. *Acc. Chem. Res.* **2020**, *53* (6), 1161−1175.

(20) Du, Y.; Yuan, X.; Sun, W.; Hu, B. Thermodynamic Modeling of the Al-K System. *J. Min. Metall. Sect. B Metall.* **2009**, *45* (1), 89−93.

(21) Hundekar, P.; Basu, S.; Fan, X.; Li, L.; Yoshimura, A.; Gupta, T.; Sarbada, V.; Lakhnot, A.; Jain, R.; Narayanan, S.; Shi, Y.; Wang, C.; Koratkar, N. In Situ Healing of Dendrites in a Potassium Metal Battery. *Proc. Natl. Acad. Sci. U.S.A.* **2020**, *117* (11), 5588−5594.

(22) Lin, T.-C.; Yang, Y.-C.; Tuan, H.-Y. Optimized K^+ Deposition Dynamics via Potassiphilic Porous Interconnected Mediators Coordinated by Single-Atom Iron for Dendrite-Free Potassium Metal Batteries. *Adv. Sci.* **2025**, *12* (8), No. 2413804.

(23) Han, W.; Liu, Y.; Meng, W.; Wang, L.; Liu, S. Dendrite-Free and Gasless Potassium Metal Anodes Assisted by the Mechanical-Electrochemical Enhancing Solid K-Electrode and Electrolyte Interface. *Chem. Eng. Sci.* **2023**, *282*, No. 119295.

(24) Gu, M.; Zhou, X.; Yang, Q.; Chu, S.; Li, L.; Li, J.; Zhao, Y.; Hu, X.; Shi, S.; Chen, Z.; Zhang, Y.; Chou, S.; Lei, K. Anion-reinforced Solvation Structure Enables Stable Operation of Ether-based Electrolyte in High-voltage Potassium Metal Batteries. *Angew. Chem.* **2024**, *136* (30), No. e202402946.

(25) Liu, T.; Shi, P.; Gao, Y.; Chen, J.; Cheng, X.; Tao, X.; Sun, Z.; Huang, F.; Jiang, Y. Regulating Interfacial Chemistry toward Highly Reversible Potassium-Metal Anodes in Carbonate Electrolytes. *J. Energy Chem.* **2025**, *111*, 211−219.

(26) Han, Y.; He, P.; Xu, Y. Energetic and Dynamic Principles of Potassium Electrodeposition in Potassium Metal Batteries. *Joule* **2025**, *9* (8), No. 102053.

(27) Wang, S.; Yan, Y.; Xiong, D.; Li, G.; Wang, Y.; Chen, F.; Chen, S.; Tian, B.; Shi, Y. Towards Dendrite-free Potassium-metal Batteries: Rational Design of a Multifunctional 3D Polyvinyl Alcohol-borax Layer. *Angew. Chem., Int. Ed.* **2021**, *60* (47), 25122−25127.

(28) Sun, J.; Du, Y.; Liu, Y.; Yan, D.; Li, X.; Ha Kim, D.; Lin, Z.; Zhou, X. Recent Advances in Potassium Metal Batteries: Electrodes, Interfaces and Electrolytes. *Chem. Soc. Rev.* **2025**, *54* (5), 2543−2594.

(29) Yuan, Z.; Liao, J.; Song, L.; Chen, A.; Su, J.; Wang, J.; Zhou, X. Entropy-Repaired Solvation Structure Strategy for High-Efficiency Phosphate-Based Localized High-Concentration Electrolytes in Potassium Batteries. *Angew. Chem.* **2025**, *137* (5), No. e202415923.

(30) Zhang, L.; Xu, J.; Li, L.; Fei, H.; Wu, Q.; Yu, H.; Yan, L.; Shu, J.; Zhang, L. Construction of KF-Rich Solid Electrolyte Interfaces Based on the Electrodeposition Behavior of FEC Additives for Protecting K-Metal Anodes. *Adv. Energy Mater.* **2025**, *15* (26), No. 2500434.

(31) Zhao, L.-K.; Zhou, J.-L.; Gao, X.-W.; Wang, X.; Bian, Y.; Liu, Z.; Gu, Q.; Luo, W.-B. Antimony Trifluoride-Engineered Hybrid Artificial Interphase Enable Dendrite-Free Potassium Metal Batteries. *Adv. Funct. Mater.* **2025**, No. 2502838.

https://doi.org/10.1021/acsaem.5c02661
ACS Appl. Energy Mater. XXXX, XXX, XXX−XXX

(32) Wang, Y.; Xu, L.; Chen, X.; Chen, Z.; Li, X.; Guo, W.; Cheng, T.; Yi, Y.; Sun, J. A Thermally Robust Biopolymeric Separator Conveys K^+ Transport and Interfacial Chemistry for Longevous Potassium Metal Batteries. *ACS Nano* **2025**, *19* (3), 3920−3930.
(33) Lu, Z.; Qiu, P.; Zhai, H.; Zhang, G.-G.; Chen, X.-W.; Lu, Z.; Wu, Y.; Chen, X. Facile Synthesis of Potassium Decahydrido-Monocarba-Closo-Decaborate Imidazole Complex Electrolyte for All-Solid-State Potassium Metal Batteries. *Angew. Chem.* **2024**, *136* (51), No. e202412401.
(34) Lyu, W.; Yu, X.; Lv, Y.; Rao, A. M.; Zhou, J.; Lu, B. Building Stable Solid-state Potassium Metal Batteries. *Adv. Mater.* **2024**, *36* (24), No. 2305795.
(35) Zhao, L.-K.; Gao, X.-W.; Ren, T.-Z.; Wang, D.; Wang, D.-W.; Liu, Z.-M.; Chen, H.; Luo, W.-B. Regulating Ion Transport Behaviors toward Dendrite-Free Potassium Metal Batteries: Recent Advances and Perspectives. *Rare Met.* **2024**, *43* (4), 1435−1460.
(36) Teng, W.; Wu, J.; Liang, Q.; Deng, J.; Xu, Y.; Liu, Q.; Wang, B.; Ma, T.; Nan, D.; Liu, J.; Li, B.; Weng, Q.; Yu, X. Designing Advanced Liquid Electrolytes for Alkali Metal Batteries: Principles, Progress, and Perspectives. *Energy Environ. Mater.* **2023**, *6* (2), No. e12355.
(37) Wang, L.; Zhang, S.; Li, N.; Chen, J.; Chen, Y.; Zhang, Z.; Tan, L.; Niu, X.; Yang, Y.; Zhang, J.; Li, H.; Ji, X.; Zhu, Y. Prospects and Challenges of Practical Nonaqueous Potassium-Ion Batteries. *Adv. Funct. Mater.* **2024**, *34* (49), No. 2408965.
(38) Chen, Y.; Wen, J.; Yi, X.; Fan, L.; Zhou, J.; Lu, B. Design Strategies for Dendrite-Free Potassium Metal Batteries. *Batteries Supercaps* **2025**, *8* (10), No. 2500106.
(39) Cao, K.; Ma, J.; Yue, Z.; Li, H.; Fan, Y.; Liu, H. Status and Challenges of Solid-State Electrolytes for Potassium Batteries. *Small* **2025**, No. 2500762.
(40) Wang, T.; Yu, Q.; Li, Z.; Gao, Y.; Huang, H.; Dong, C.; Yang, C.; Chong, S.; Wang, W.; Zhang, J. The Potential of Solid-State Potassium-Ion Batteries with Polymer-Based Electrolytes. *Carbon Energy* **2025**, *7* (3), No. e670.
(41) Li, P.; Xu, T.; Ding, P.; Deng, J.; Zha, C.; Wu, Y.; Wang, Y.; Li, Y. Highly Reversible Na and K Metal Anodes Enabled by Carbon Paper Protection. *Energy Storage Mater.* **2018**, *15*, 8−13.
(42) Zhou, R.; Tan, H.; Gao, Y.; Hou, Z.; Du, X.; Zhang, B. Constructing Resilient Solid Electrolyte Interphases on Carbon Nanofiber Film for Advanced Potassium Metal Anodes. *Carbon* **2022**, *186*, 141−149.
(43) Yang, Y.; Huang, C.; Zhang, Y.; Wu, Y.; Zhao, X.; Qian, Y.; Chang, G.; Tang, Q.; Hu, A.; Chen, X. Processable Potassium−Carbon Nanotube Film with a Three-Dimensional Structure for Ultrastable Metallic Potassium Anodes. *ACS Appl. Mater. Interfaces* **2022**, *14* (50), 55577−55586.
(44) Lei, Y.; Zhang, S.; Dong, J.; Gao, Y.; Gao, C.; Wei, Y.; Qin, L.; Han, D.; Huang, D.; Wei, G.; Zhai, D.; Kang, F. Potassium-Enriched Graphite for Use as Stable Hybrid Anodes in High-Efficiency Potassium Batteries. *Carbon* **2023**, *201*, 1030−1037.
(45) Wang, Z.; Wu, J.-F.; Zhou, W.; Mo, Y.; Chen, S.; Zhou, T.; Shen, W.; Ren, B.; Huang, P.; Liu, J. Ultrathin K−C Composite Anode Enables Conformal Stripping/Plating for Dendrite-Free and High-Rate Potassium-Metal Batteries. *ACS Energy Lett.* **2024**, *9* (9), 4534−4543.
(46) Qin, L.; Lei, Y.; Wang, H.; Dong, J.; Wu, Y.; Zhai, D.; Kang, F.; Tao, Y.; Yang, Q. Capillary Encapsulation of Metallic Potassium in Aligned Carbon Nanotubes for Use as Stable Potassium Metal Anodes. *Adv. Energy Mater.* **2019**, *9* (29), No. 1901427.
(47) Wang, H.; Hu, J.; Dong, J.; Lau, K. C.; Qin, L.; Lei, Y.; Li, B.; Zhai, D.; Wu, Y.; Kang, F. Artificial Solid-electrolyte Interphase Enabled High-capacity and Stable Cycling Potassium Metal Batteries. *Adv. Energy Mater.* **2019**, *9* (43), No. 1902697.
(48) Liu, Y.; Shi, Y.; Gao, C.; Shi, Z.; Ding, H.; Feng, Y.; He, Y.; Sha, J.; Zhou, J.; Lu, B. Low-temperature Potassium Batteries Enabled by Electric and Thermal Field Regulation. *Angew. Chem., Int. Ed.* **2023**, *62* (16), No. e202300016.
(49) Ding, H.; Feng, Y.; Zhou, J.; Yu, X.; Fan, L.; Lu, B. Superstable Potassium Metal Batteries with a Controllable Internal Electric Field. *Fundam. Res.* **2023**, *3* (5), 813−821.
(50) Yuan, W.; Zhang, T.; Mou, P.; Chen, Y.; Shu, J.; Zhang, L. Establishing Non-Newtonian Flow State K Metal Electrodes for Flexible Batteries. *Energy Storage Mater.* **2023**, *61*, No. 102895.
(51) Chen, X.; Bai, Y.-K.; Shen, X.; Peng, H.-J.; Zhang, Q. Sodiophilicity/Potassiophilicity Chemistry in Sodium/Potassium Metal Anodes. *J. Energy Chem.* **2020**, *51*, 1−6.
(52) Xiong, J.; Ye, M.; Wang, Z.; Chen, J.; Zhang, Y.; Tang, Y.; Li, C. C. Fast and Homogeneous Ion Regulation toward a 4 V, High-Rate and Dendrite-Free Potassium Metal Battery. *Chem. Eng. J.* **2022**, *442*, No. 135927.
(53) Meng, J.; Zhu, H.; Xiao, Z.; Zhang, X.; Niu, C.; Liu, Y.; Jiang, G.; Wang, X.; Qiao, F.; Hong, X.; Liu, F.; Pang, Q.; Mai, L. Amine-Wetting-Enabled Dendrite-Free Potassium Metal Anode. *ACS Nano* **2022**, *16* (5), 7291−7300.
(54) Zhou, M.; Qi, W.; Hu, Z.; Cheng, M.; Zhao, X.; Xiong, P.; Su, H.; Li, M.; Hu, J.; Xu, Y. Highly Potassiophilic Carbon Nanofiber Paper Derived from Bacterial Cellulose Enables Ultra-Stable Dendrite-Free Potassium Metal Anodes. *ACS Appl. Mater. Interfaces* **2021**, *13* (15), 17629−17638.
(55) Liu, P.; Wang, Y.; Gu, Q.; Nanda, J.; Watt, J.; Mitlin, D. Dendrite-free Potassium Metal Anodes in a Carbonate Electrolyte. *Adv. Mater.* **2020**, *32* (7), No. 1906735.
(56) Wei, Z.; Wang, A.; Guan, X.; Li, G.; Yang, Z.; Huang, C.; Zhang, J.; Ren, L.; Luo, J.; Liu, X. Processable Potassium Metal Anode for Stable Batteries. *Energy Environ. Mater.* **2022**, *5* (4), 1278−1284.
(57) Luo, T.; Zhao, Q.; Liu, Y.; Meng, W.; Sun, Q.; Dai, L.; Liu, S.; Wang, L. High-rate and Dendrite-free Liquid Alloy Anode for High Energy Potassium Metal Batteries. *Ecomat* **2022**, *4* (5), No. e12203.
(58) Sun, J.; Duan, L.; Yuan, Z.; Li, X.; Yan, D.; Zhou, X. Hydroxyl-decorated Carbon Cloth with High Potassium Affinity Enables Stable Potassium Metal Anodes. *Small* **2024**, *20* (11), No. 2311314.
(59) Li, Z.; Ma, L.; Han, K.; Ji, Y.; Xie, J.; Pan, L.; Li, J.; Mai, W. A Host Potassiophilicity Strategy for Unprecedentedly Stable and Safe K Metal Batteries. *Chem. Sci.* **2023**, *14* (34), 9114−9122.
(60) Liu, P.; Yen, D.; Vishnugopi, B. S.; Kankanallu, V. R.; Gürsoy, D.; Ge, M.; Watt, J.; Mukherjee, P. P.; Chen-Wiegart, Y. K.; Mitlin, D. Influence of Potassium Metal-support Interactions on Dendrite Growth. *Angew. Chem.* **2023**, *135* (23), No. e202300943.
(61) Shen, X.; Sun, H.; Li, B.; Yuan, Y.; Zhang, L.; Li, S.; Wang, L.; Lu, B.; Zhu, J.; Duan, X. Dual-Strategy Coupling Driven Versatile Carbon-Based Anode for Potassium-Ion/Potassium Metal Storage. *Chem. Eng. J.* **2023**, *473*, No. 145155.
(62) Chen, Z.; Wang, L.; Zheng, J.; Huang, Y.; Huang, H.; Li, C.; Shao, Y.; Wu, X.; Rui, X.; Tao, X.; Yang, H.; Yu, Y. Unraveling the Nucleation and Growth Mechanism of Potassium Metal on 3D Skeletons for Dendrite-Free Potassium Metal Batteries. *ACS Nano* **2024**, *18* (11), 8496−8510.
(63) Zhang, J.; Li, Y.; Zhu, L.; Wang, X.; Tu, J. Potassiophilic Skeleton Achieving Highly Stable Potassium Metal Anode. *Chem. Eng. J.* **2022**, *449*, No. 137659.
(64) Zhang, J.; Cai, D.; Zhu, L.; Wang, X.; Tu, J. Highly Stable Potassium Metal Anodes with Controllable Thickness and Area Capacity. *Small* **2023**, *19* (34), No. 2301119.
(65) Li, H.; Liu, Y.; Wang, J.; Yan, W.; Zhang, J. Robust 3D Copper Foam Functionalized with Gold Nanoparticles as Anode for High-performance Potassium Metal Batteries. *Chem. - Asian J.* **2022**, *17* (15), No. e202200430.
(66) Wang, J.; Yan, W.; Zhang, J. High Area Capacity and Dendrite-Free Anode Constructed by Highly Potassiophilic Pd/Cu Current Collector for Low-Temperature Potassium Metal Battery. *Nano Energy* **2022**, *96*, No. 107131.
(67) Ren, N.; Wang, L.; Li, X.; Cao, K.; He, Z.; Shao, Y.; Xiao, J.; Zhu, Y.; Pan, B.; Jiao, S.; Chen, C. Design Principles of Mediation Layer for Current Collectors toward High-performance Anode-free Potassium-metal Batteries: A Case Study of Cu_6Sn_5 on Copper. *Adv. Funct. Mater.* **2024**, *34* (23), No. 2313538.

https://doi.org/10.1021/acsaem.5c02661
ACS Appl. Energy Mater. XXXX, XXX, XXX−XXX

(68) Wang, J.; Yuan, J.; Chen, C.; Wang, L.; Zhai, Z.; Fu, Q.; Liu, Y.; Dong, L.; Yan, W.; Li, A.; Zhang, J. Cu_3Pt Alloy-Functionalized Cu Mesh as Current Collector for Dendritic-Free Anodes of Potassium Metal Batteries. *Nano Energy* **2020**, *75*, No. 104914.
(69) Song, S.; Wang, L.; Xie, S.; Zhang, Q.; Lu, B. Fabricating Potassiophilic Alloy Anode with Liquid Metal Enables Superior Potassium Ion Deposition. *ACS Appl. Mater. Interfaces* **2025**, *17* (22), 32445−32455.
(70) Chang, C.; Tseng, Y.; Lu, Y.; Yang, Y.; Tuan, H. High Entropy Induced Local Charge Enhancement Promotes Frank−Van Der Merwe Growth for Dendrite-free Potassium Metal Batteries. *Adv. Funct. Mater.* **2024**, *34* (52), No. 2411193.
(71) Zhao, L.; Gao, X.; Mu, J.; Luo, W.; Liu, Z.; Sun, Z.; Gu, Q.; Li, F. Durable Integrated K-metal Anode with Enhanced Mass Transport through Potassiphilic Porous Interconnected Mediator. *Adv. Funct. Mater.* **2023**, *33* (41), No. 2304292.
(72) Shen, Q.; He, Y.; Wang, J. Biomass-Derived Two-Dimensional N,O-Doped Carbon with Embedded Binary-Metal Nanoparticles Enables Dendrite-Free Potassium-Metal Anodes. *J. Mater. Chem. A* **2023**, *11* (18), 9829−9839.
(73) Cheng, G.; Liu, S.; Wang, X.; Li, X.; Su, Y.; Shi, J.; Huang, M.; Shi, Z.; Wang, H.; Yan, Z. CoZn Nanoparticles@hollow Carbon Tubes Enabled High-Performance Potassium Metal Batteries. *ACS Appl. Mater. Interfaces* **2022**, *14* (40), 45364−45372.
(74) Yi, Y.; Li, J.; Gao, Z.; Liu, W.; Zhao, Y.; Wang, M.; Zhao, W.; Han, Y.; Sun, J.; Zhang, J. Highly Potassiophilic Graphdiyne Skeletons Decorated with Cu Quantum Dots Enable Dendrite-free Potassium-metal Anodes. *Adv. Mater.* **2022**, *34* (29), No. 2202685.
(75) Zhang, D.; Ma, X.; Wu, L.; Wen, J.; Li, F.; Zhou, J.; Rao, A. M.; Lu, B. Coupling Low-tortuosity Carbon Matrix with Single-atom Chemistry Enables Dendrite-free Potassium-metal Anode. *Adv. Energy Mater.* **2023**, *13* (2), No. 2203277.
(76) Tseng, Y.-Y.; Tuan, H.-Y. Coherent Single-Atom Dipole−Dipole Coupling Mediates Holistic Regulation of K^+ Migration for Superior Energy Storage and Dendrite-Free Metal Deposition. *Adv. Funct. Mater.* **2025**, *35* (31), No. 2423387.
(77) Liu, Q.; Mu, Y.; Ye, T.; Lian, X.; Su, Y.; Chen, X.; Shi, Z.; Meng, Z.; Zeng, L.; Sun, Z.; Sun, J. Transition Metal Atom−Cluster Synergistic Modification with Tuned d-Band Center Imparts Longevous Potassium Metal Anodes. *Angew. Chem., Int. Ed.* **2025**, *64* (34), No. e202510150.
(78) Song, L.; Li, R.; Liao, W.; Sun, J.; Li, X.; Xu, Y.; Zhou, G.; Zhou, X. A Flexible and Potassiphilic Porous Interconnected Mediator for Dendrite-Free and Stable Potassium Metal Anodes. *Energy Storage Mater.* **2024**, *71*, No. 103643.
(79) Oliveira, Y. L.; Gouveia, A. F.; Costa, M. J. S.; Lopes, F. H. P.; Sczancoski, J. C.; Longo, E.; Luz, G. E., Jr.; Santos, R. S.; Cavalcante, L. S. Investigation of Electronic Structure, Morphological Features, Optical, Colorimetric, and Supercapacitor Electrode Properties of $CoWO_4$ Crystals. *Mater. Sci. Energy Technol.* **2022**, *5*, 125−144.
(80) Fei, Y.; Jiang, J.; Zhang, L.; Nie, P.; Jiang, Y.; Chen, Y.; Zhuang, Q.; Ju, Z. Potassiophilic α-MoC Anchored on 3D Carbon Host Enables Uniform Potassium Nucleation and Super-Stable Potassium Metal Anodes. *Chem. Eng. J.* **2024**, *490*, No. 151527.
(81) dos Santos Politi, J. R.; Viñes, F.; Rodriguez, J. A.; Illas, F. Atomic and Electronic Structure of Molybdenum Carbide Phases: Bulk and Low Miller-Index Surfaces. *Phys. Chem. Chem. Phys.* **2013**, *15* (30), 12617−12625.
(82) Wang, H.-W.; Naguib, M.; Page, K.; Wesolowski, D. J.; Gogotsi, Y. Resolving the Structure of $Ti_3C_2T_x$ MXenes through Multilevel Structural Modeling of the Atomic Pair Distribution Function. *Chem. Mater.* **2016**, *28* (1), 349−359.
(83) Lashgari, H.; Abolhassani, M. R.; Boochani, A.; Elahi, S. M.; Khodadadi, J. Electronic and Optical Properties of 2D Graphene-like Compounds Titanium Carbides and Nitrides: DFT Calculations. *Solid State Commun.* **2014**, *195*, 61−69.
(84) Shi, H.; Dong, Y.; Zheng, S.; Dong, C.; Wu, Z.-S. Three Dimensional Ti_3C_2 MXene Nanoribbon Frameworks with Uniform Potassiophilic Sites for the Dendrite-Free Potassium Metal Anodes. *Nanoscale Adv.* **2020**, *2* (9), 4212−4219.
(85) Tang, X.; Zhou, D.; Li, P.; Guo, X.; Sun, B.; Liu, H.; Yan, K.; Gogotsi, Y.; Wang, G. MXene-Based Dendrite-Free Potassium Metal Batteries. *Adv. Mater.* **2020**, *32* (4), No. 1906739.
(86) Magne, D.; Mauchamp, V.; Célérier, S.; Chartier, P.; Cabioc'h, T. Site-Projected Electronic Structure of Two-Dimensional Ti_3C_2 MXene: The Role of the Surface Functionalization Groups. *Phys. Chem. Chem. Phys.* **2016**, *18* (45), 30946−30953.
(87) Chen, Y.; Liu, Z.; Lu, Y.; Gao, X.-W.; Zhou, J.-L.; Wang, X.-C.; Gu, Q.-F.; Luo, W.-B. Uniform Potassium Metal Deposition under Fast Ion Transportation Kinetic: Porous Carbon Nanotube/Metal−Organic Frameworks Composite Host. *J. Power Sources* **2024**, *613*, No. 234909.
(88) Cheng, G.; Liu, S.; Su, Y.; Wang, X.; Li, X.; Shi, J.; Huang, M.; Shi, Z.; Wang, H. Bi@hollow Carbon Tube Enabled High Performance Potassium Metal Batteries. *J. Alloys Compd.* **2022**, *913*, No. 165329.
(89) Zhang, D.-T.; Liu, M.-C.; Li, M.-P.; Yuan, Z.-Z.; Hu, Y.-X.; Chen, H.; Li, C.-Y.; Kong, L.-B.; Zhao, K.; Ren, J.-Q.; Liu, B. One-Stone, Two Birds: Three-Dimensional Structure and Rich-Inorganic Solid Electrolyte Interface Derived from Bi Nanoparticles Modified Ti_3C_2/CNT/rGO Aerogel for Anode-Free Potassium Metal Batteries. *Chem. Eng. J.* **2024**, *482*, No. 148896.
(90) Ye, S.; Wang, L.; Liu, F.; Shi, P.; Yu, Y. Integration of Homogeneous and Heterogeneous Nucleation Growth via 3D Alloy Framework for Stable Na/K Metal Anode. *Escience* **2021**, *1* (1), 75−82.
(91) Shi, G.; Xie, J.; Li, Z.; Sun, P.; Yin, Y.; Pan, L.; Hui, K. N.; Mai, W.; Li, J. A Bismuth Oxide-Modified Copper Host Achieving Bubble-Free and Stable Potassium Metal Batteries. *Chem. Sci.* **2025**, *16* (3), 1344−1352.
(92) Feng, Y.; Rao, A. M.; Zhou, J.; Lu, B. Selective Potassium Deposition Enables Dendrite-resistant Anodes for Ultrastable Potassium-metal Batteries. *Adv. Mater.* **2023**, *35* (30), No. 2300886.
(93) Li, H.-Y.; Li, M.-P.; Zhang, D.-T.; Chen, H.; Li, C.-Y.; Shi, W.-J.; Xue, H.-T.; Liu, M.-C. A "Two-Pronged" Strategy towards Dendrite-Free Potassium Metal Anodes: Potassiophilic Zinc Modification Synergized with in-Situ Red Phosphorus-Derived Protective Layer. *Electrochim. Acta* **2024**, *479*, No. 143880.
(94) Xia, S.; Xu, H.; Zou, H.; Shang, M.; Li, L.; Ouyang, B.; Zhang, W. A 3D Structural NC/ZnO@carbon Cloth Matrix as a Potassiophilic Host for a Dendrite-Free Potassium Metal Anode. *Inorg. Chem. Front.* **2024**, *11* (16), 5043−5053.
(95) Li, Y.; Liang, S.; Liu, S.; Sun, Y.; Miao, J.; Lu, Y.; Qian, K.; Lv, M.; Guo, C.; Han, P.; Li, X.; Shao, W.; He, J. Synchrotron-Tailored Hierarchical Carbon Nanofibers with ZnO Decoration for Long-Lifespan Potassium Metal Batteries. *Electrochim. Acta* **2025**, *536*, No. 146726.
(96) Zhang, D.-T.; Liu, M.-C.; Li, M.-P.; Chen, H.; Li, C.-Y.; Hu, Y.-X.; Kong, L.-B.; Zhang, X.-Y.; Gu, B.-N.; Liu, M.-J.; Zhao, K.; Ren, J.-Q.; Yuan, Z.-Z.; Chueh, Y.-L. Design of a Potassiophilic 3D Conductive Scaffold Potassium Anode (3D-CTZ@K) with Dendrite-Free and High Energy-Power Density in Potassium Metal Batteries. *J. Mater. Chem. A* **2023**, *11* (38), 20741−20751.
(97) Xia, S.; Zou, H.; Zhang, Y.; Zhu, Q.; Li, L.; Zhang, W. Spontaneous Phase Separation of KF-K/KZn_{13} Achieves Durable Potassium Metal Anode. *Chem. Eng. J.* **2025**, *511*, No. 162046.
(98) Chen, X.; Zhang, M.; Jia, L.; Yi, Y.; Su, Y.; Lian, X.; Lu, M.; Zou, Y.; Chen, Z.; Wang, Y.; Gu, J.; Zhao, W.; Yang, X.; Sun, J. Alloy-Boosted Potassiophilic Membrane Interphase for Ultrastable K Metal Anodes. *Adv. Funct. Mater.* **2025**, *35* (16), No. 2421110.
(99) Li, S.; Zhu, H.; Liu, Y.; Han, Z.; Peng, L.; Li, S.; Yu, C.; Cheng, S.; Xie, J. Codoped Porous Carbon Nanofibres as a Potassium Metal Host for Nonaqueous K-Ion Batteries. *Nat. Commun.* **2022**, *13* (1), No. 4911.
(100) Ye, M.; Hwang, J.-Y.; Sun, Y.-K. A 4 V Class Potassium Metal Battery with Extremely Low Overpotential. *ACS Nano* **2019**, *13* (8), 9306−9314.

https://doi.org/10.1021/acsaem.5c02661
ACS Appl. Energy Mater. XXXX, XXX, XXX−XXX

(101) Qiao, F.; Meng, J.; Wang, J.; Wu, P.; Xu, D.; An, Q.; Wang, X.; Mai, L. Building Carbon Cloth-Based Dendrite-Free Potassium Metal Anodes for Potassium Metal Pouch Cells. *J. Mater. Chem. A* **2021**, *9* (40), 23046−23054.
(102) Zhao, X.; Chen, F.; Liu, J.; Cheng, M.; Su, H.; Liu, J.; Xu, Y. Enhanced Surface Binding Energy Regulates Uniform Potassium Deposition for Stable Potassium Metal Anodes. *J. Mater. Chem. A* **2020**, *8* (11), 5671−5678.
(103) Zhang, D.; Liu, M.; Shi, W.; Qiu, Y.; Hu, Y.; Yuan, Z.; Xue, H.; Kong, L.; Zhao, K.; Ren, J.; Liu, B. Dual-Gradient Engineering of Conductive and Hierarchically Potassiophilic Network for Highly Stable Potassium Metal Anode. *Adv. Energy Mater.* **2024**, *14* (40), No. 2401960.
(104) Han, M.; Jiang, J.; Lu, S.; Jiang, Y.; Ma, W.; Liu, X.; Zhao, B.; Zhang, J. Moderate Specific Surface Areas Help Three-Dimensional Frameworks Achieve Dendrite-Free Potassium-Metal Anodes. *ACS Appl. Mater. Interfaces* **2022**, *14* (1), 900−909.
(105) Xie, J.; Ji, Y.; Ma, L.; Wen, Z.; Pu, J.; Wang, L.; Ding, S.; Shen, Z.; Liu, Y.; Li, J.; Mai, W.; Hong, G. Bifunctional Alloy/Solid-Electrolyte Interphase Layer for Enhanced Potassium Metal Batteries via Prepassivation. *ACS Nano* **2023**, *17* (2), 1511−1521.
(106) Wu, S.; Li, H.; Jing, Z.; Wu, Y.; Yang, C.; Wang, Y. *In-Situ* Induction of Gradient Nucleation Alloy Seeds Confined in Nitrogen-Doped Carbon for Highly Efficient and Dendrite-Free Potassium Metal Batteries. *Chem. Eng. J.* **2025**, *518*, No. 164631.
(107) Zhou, J.; Zhao, L.; Lu, Y.; Gao, X.; Chen, Y.; Liu, Z.; Gu, Q.; Luo, W. Bark-inspired Functional-carbon/Potassium Composite Electrode with Fast Ion Transport Channels for Dendrite-free Potassium Metal Batteries. *Adv. Funct. Mater.* **2024**, *34* (40), No. 2403754.
(108) Qi, J.; Lin, C.; Deng, S.; Zuo, Y.; Zheng, H.; Jiao, X.; Yan, W.; Zhang, J. Synergy of Cu-Foam/Sb_2O_3/rGO for Stable Potassium Anodes of High-Rate and Low-Temperature Potassium Metal Batteries. *J. Mater. Chem. A* **2024**, *12* (12), 6968−6982.
(109) Sun, Z.; Liu, M.; Liu, B.; Khan, R.; Zhao, J.; Huang, L.; Wu, Y. Dynamically Evolving Multifunctional Protective Layer for Highly Stable Potassium Metal Anodes. *ACS Appl. Mater. Interfaces* **2023**, *15* (50), 58429−58436.
(110) Yang, Q.; Ding, Y.; He, G. An Amalgam Route to Stabilize Potassium Metal Anodes over a Wide Temperature Range. *Chem. Commun.* **2020**, *56* (24), 3512−3515.
(111) Cui, Z.; Song, J.; Chen, M.; Wang, W.; Zhang, W.; Zhu, Q. Non-Completely Selenized Cu-OSe Nanowires as Potassium-Philic Host for Anode-Free Potassium Metal Batteries. *Energy Storage Mater.* **2024**, *71*, No. 103649.
(112) Jiang, J.; Liu, Y.; Liao, Y.; Li, W.; Xu, Y.; Liu, X.; Jiang, Y.; Zhang, J.; Zhao, B. Construction of Synchronous-deposition K Metal Anodes via Modulation of Ion/Electron Transport Kinetics for High-rate and Low-temperature K Metal Batteries. *Small* **2023**, *19* (32), No. 2300854.
(113) Lei, Y.; Chen, M.; Li, Y.; Zhang, W.; Zhao, D.; Zhu, Q. Dendrite-Free Potassium Metal Anode Induced by In-Situ Phase Transitions of MoS_2. *Mater. Today Phys.* **2023**, *35*, No. 101141.
(114) Liu, S.; Yang, Y.; Qian, Y.; Chang, G.; Zhao, X.; Tang, Q.; Hu, A.; Chen, X. MOF-derived Potassiophilic CuO Nanoparticles on Carbon Fiber Cloth as Host for Stabilizing Potassium Metal Anode. *ChemElectroChem* **2022**, *9* (3), No. e202101561.
(115) Li, X.; Sun, J.; Song, L.; Jiang, X.; Mo, X.; Shen, J.; Zhou, X. Nanomesh NiO-Modified Carbon Cloth for Highly Efficient Self-Supporting Potassium Metal Anodes. *Chem. Eng. J.* **2024**, *490*, No. 151521.
(116) Li, Y.; Zhang, L.; Liu, S.; Wang, X.; Xie, D.; Xia, X.; Gu, C.; Tu, J. Original Growth Mechanism for Ultra-Stable Dendrite-Free Potassium Metal Electrode. *Nano Energy* **2019**, *62*, 367−375.
(117) Zhang, D.-T.; Shi, W.-J.; Li, M.-P.; Chen, H.; Li, C.-Y.; Hu, Y.-X.; Kong, L.-B.; Zhao, K.; Ren, J.-Q.; Xue, H.-T.; Yuan, Z.-Z.; Liu, M.-C. Orderly Arranged Three-Dimensional Porous S/Ti_3C_2/NC Potassiphilic Scaffold Enabling Dendrite-Free K Metal Deposition for Potassium Metal Batteries. *J. Energy Storage* **2024**, *77*, No. 109903.
(118) Li, M.-P.; Li, H.-Y.; Shi, W.-J.; Wang, X.-R.; Xue, H.-T.; Ren, J.-Q.; Zhao, K.; Liu, B.; Kong, L.-B.; Liu, M.-C. Enhanced Potassium Ion Diffusion and Interface Stability Enabled by Potassiophilic rGO/CNTs/NaF Micro-Lattice Aerogel for High-Performance Potassium Metal Batteries. *Adv. Funct. Mater.* **2025**, No. e08586.
(119) Lian, X.; Ju, Z.; Li, L.; Yi, Y.; Zhou, J.; Chen, Z.; Zhao, Y.; Tian, Z.; Su, Y.; Xue, Z.; Chen, X.; Ding, Y.; Tao, X.; Sun, J. Dendrite-free and High-rate Potassium Metal Batteries Sustained by an Inorganic-rich SEI. *Adv. Mater.* **2024**, *36* (9), No. 2306992.
(120) Yu, Z.; Liu, Q.; Wang, D.; Shi, J.; Zhai, D.; Zhang, B. Unraveling Electrode Surface Chemistry in Determining Interphase Stability and Deposition Homogeneity for Anode-Free Potassium Metal Batteries. *Angew. Chem., Int. Ed.* **2025**, *64* (22), No. e202502091.
(121) Zhang, X.-L.; Ma, L.; Cai, Y.-P.; Fransaer, J.; Zheng, Q. A Low-Fermi-Level Current Collector Enables Anode-Free Lithium Metal Batteries with Long Cycle Life. *Matter* **2024**, *7* (2), 583−602.
(122) Song, L.; Yang, Q.; Yao, Y.; Tan, M.; Li, R.; Liao, J.; Zhou, X.; Yu, Y. Surface Work Function-Induced High-Entropy Solid Electrolyte Interphase Formation for Highly Stable Potassium Metal Anodes. *Angew. Chem., Int. Ed.* **2025**, *64* (29), No. e202509252.
(123) Garrillo, P. A. F.; Grévin, B.; Chevalier, N.; Borowik, Ł. Calibrated Work Function Mapping by Kelvin Probe Force Microscopy. *Rev. Sci. Instrum.* **2018**, *89* (4), No. 043702.
(124) Zandvliet, H. J. W.; van Houselt, A. Scanning Tunneling Spectroscopy. *Annu. Rev. Anal. Chem.* **2009**, *2*, 37−55.
(125) Wang, Y.; Yang, X.; Meng, Y.; Wen, Z.; Han, R.; Hu, X.; Sun, B.; Kang, F.; Li, B.; Zhou, D.; Wang, C.; Wang, G. Fluorine Chemistry in Rechargeable Batteries: Challenges, Progress, and Perspectives. *Chem. Rev.* **2024**, *124* (6), 3494−3589.
(126) Li, G.-X.; Lennartz, P.; Koverga, V.; Kou, R.; Nguyen, A.; Jiang, H.; Liao, M.; Wang, D.; Dandu, N.; Zepeda, M.; Wang, H.; Wang, K.; Ngo, A. T.; Brunklaus, G.; Wang, D. Interfacial Solvation-Structure Regulation for Stable Li Metal Anode by a Desolvation Coating Technique. *Proc. Natl. Acad. Sci. U.S.A.* **2024**, *121* (4), No. e2311732121.
(127) Heng, Y.-L.; Gu, Z.-Y.; Liu, H.-H.; Liang, H.-J.; Deng, Y.; Zhao, J.; Wang, X.-T.; Xue, Z.-H.; Lü, H.-Y.; Wu, X.-L. Breaking Anionic Solvation Barrier for Safe and Durable Potassium-Ion Batteries under Ultrahigh-Voltage Operation. *Angew. Chem., Int. Ed.* **2025**, *64* (14), No. e202423044.
(128) Cheng, C.; Zhou, Y.; Xu, Y.; Jia, H.; Kim, J.; Xu, W.; Wang, C.; Gao, P.; Zhu, Z. Dynamic Molecular Investigation of the Solid-Electrolyte Interphase of an Anode-Free Lithium Metal Battery Using In Situ Liquid SIMS and Cryo-TEM. *Nano Lett.* **2023**, *23* (18), 8385−8391.
(129) Adenusi, H.; Chass, G. A.; Passerini, S.; Tian, K. V.; Chen, G. Lithium Batteries and the Solid Electrolyte Interphase (SEI)—Progress and Outlook. *Adv. Energy Mater.* **2023**, *13* (10), No. 2203307.
(130) Zhang, X.; Guo, Z.; Li, X.; Liu, Q.; Hu, H.; Li, F.; Huang, Q.; Zhang, L.; Tang, Y.; Huang, J. Cryo-Ultramicrotomy Enables TEM Characterization of Global Lithium/Polymer Interfaces. *Energy Environ. Sci.* **2024**, *17* (4), 1436−1447.
(131) Li, Z.; Wang, L.; Huang, X.; He, X. Unveiling the Mystery of LiF within Solid Electrolyte Interphase in Lithium Batteries. *Small* **2024**, *20* (22), No. 2305429.
(132) Rahman, M. M.; Tan, S.; Yang, Y.; Zhong, H.; Ghose, S.; Waluyo, I.; Hunt, A.; Ma, L.; Yang, X.-Q.; Hu, E. An Inorganic-Rich but LiF-Free Interphase for Fast Charging and Long Cycle Life Lithium Metal Batteries. *Nat. Commun.* **2023**, *14* (1), No. 8414.
(133) Wi, T.-U.; Park, S. O.; Yeom, S. J.; Kim, M.-H.; Kristanto, I.; Wang, H.; Kwak, S. K.; Lee, H.-W. Revealing the Dual-Layered Solid Electrolyte Interphase on Lithium Metal Anodes via Cryogenic Electron Microscopy. *ACS Energy Lett.* **2023**, *8* (5), 2193−2200.
(134) Sayahpour, B.; Li, W.; Bai, S.; Lu, B.; Han, B.; Chen, Y.-T.; Deysher, G.; Parab, S.; Ridley, P.; Raghavendran, G.; Bao Nguyen, L. H.; Zhang, M.; Shirley Meng, Y. Quantitative Analysis of Sodium

https://doi.org/10.1021/acsaem.5c02661
ACS Appl. Energy Mater. XXXX, XXX, XXX−XXX

Metal Deposition and Interphase in Na Metal Batteries. *Energy Environ. Sci.* **2024**, *17* (3), 1216−1228.
(135) Wang, K.; Kim, J. T.; Yuan, X.; Kim, J. K.; Liu, B.; Kim, M.; Zhao, D.; Mecklenburg, M.; Li, Y. Trapping and Imaging Dynamic Battery Nanointerfaces via Electrified Cryo-EM. *Sci. Adv.* **2025**, *11* (24), No. eadv3191.
(136) Hu, T.; Huang, H.; Zhou, G.; Wang, X.; Zhu, J.; Cheng, Z.; Fu, F.; Wang, X.; Dai, F.; Yu, K.; Xu, S. Observation of Dendrite Formation at Li Metal-Electrolyte Interface by a Machine-Learning Enhanced Constant Potential Framework. *Nat. Commun.* **2025**, *16* (1), No. 7379.
(137) Lai, G.; Zuo, Y.; Fang, C.; Huang, Z.; Chen, T.; Liu, Q.; Cui, S.; Zheng, J. Unraveling Charge Effects on Interface Reactions and Dendrite Growth in Lithium Metal Anode. *Npj Comput. Mater.* **2025**, *11* (1), No. 121.
(138) Severson, K. A.; Attia, P. M.; Jin, N.; Perkins, N.; Jiang, B.; Yang, Z.; Chen, M. H.; Aykol, M.; Herring, P. K.; Fraggedakis, D.; Bazant, M. Z.; Harris, S. J.; Chueh, W. C.; Braatz, R. D. Data-Driven Prediction of Battery Cycle Life before Capacity Degradation. *Nat. Energy* **2019**, *4* (5), 383−391.
(139) Jia, Q.; Liu, H.; Wang, X.; Tao, Q.; Zheng, L.; Li, J.; Wang, W.; Liu, Z.; Gu, X.; Shen, T.; Hou, S.; Jin, Z.; Ma, J. Machine Learning-Driven Mass Discovery and High-Throughput Screening of Fluoroether-Based Electrolytes for High-Stability Lithium Metal Batteries. *Angew. Chem., Int. Ed.* **2025**, *64* (17), No. e202424493.
(140) Cho, B.-K.; Jung, S.-Y.; Park, S.-J.; Hyun, J.-H.; Yu, S.-H. In Situ/Operando Imaging Techniques for next-Generation Battery Analysis. *ACS Energy Lett.* **2024**, *9* (8), 4068−4092.
(141) Zhang, Q.; Han, B.; Zou, Y.; Shen, S.; Li, M.; Lu, X.; Wang, M.; Guo, Z.; Yao, J.; Chang, Z.; Gu, M. Enabling Atomic-Scale Imaging of Sensitive Potassium Metal and Related Solid Electrolyte Interphases Using Ultralow-Dose Cryo-TEM. *Adv. Mater.* **2021**, *33* (43), No. 2102666.
(142) Yun, D.-J.; Kim, S.; Heo, S.; Choi, H.; Baik, J.; Chung, J.; Park, S.; Yu, D.; Lee, J.; Kang, S.; Jung, C.; Ko, D.-S. Understanding the Role of Metal Interlayers in All-Solid-Electrolyte Batteries Using Operando X-Ray Photoelectron Spectroscopy. *Adv. Energy Mater.* **2024**, *14* (34), No. 2401473.
(143) Sukumaran, S.; Fearn, S.; Skinner, S. J. In Situ TOF-SIMS Investigation of the Dynamic Metallic Anodelsolid Electrolyte Interface in Solid-State Sodium-Ion Batteries. *Cell Rep. Phys. Sci.* **2025**, *6* (2), No. 102447.
(144) Wang, S.; Shi, H.; Wang, D.; Xia, Y.; Yin, Y.; Liang, S.; Hu, Y.; Shao, R.; Wu, X.; Xu, Z. Neutron-Based Characterization: A Rising Star in Illuminating Rechargeable Lithium Metal Batteries. *Nano Energy* **2024**, *122*, No. 109337.
(145) Lin, X.; Shen, Y.; Yu, Y.; Huang, Y. In Situ NMR Verification for Stacking Pressure-Induced Lithium Deposition and Dead Lithium in Anode-Free Lithium Metal Batteries. *Adv. Energy Mater.* **2024**, *14* (14), No. 2303918.
(146) Liu, P.; Yang, L.; Xiao, B.; Wang, H.; Li, L.; Ye, S.; Li, Y.; Ren, X.; Ouyang, X.; Hu, J.; Pan, F.; Zhang, Q.; Liu, J. Revealing Lithium Battery Gas Generation for Safer Practical Applications. *Adv. Funct. Mater.* **2022**, *32* (47), No. 2208586.
(147) Drvarič Talian, S.; Kapun, G.; Moškon, J.; Dominko, R.; Gaberšček, M. Operando Impedance Spectroscopy with Combined Dynamic Measurements and Overvoltage Analysis in Lithium Metal Batteries. *Nat. Commun.* **2025**, *16* (1), No. 2030.
(148) Xiao, J.; Li, Q.; Bi, Y.; Cai, M.; Dunn, B.; Glossmann, T.; Liu, J.; Osaka, T.; Sugiura, R.; Wu, B.; Yang, J.; Zhang, J.-G.; Whittingham, M. S. Understanding and Applying Coulombic Efficiency in Lithium Metal Batteries. *Nat. Energy* **2020**, *5* (8), 561−568.
(149) Zhao, J.; Feng, X.; Tran, M.-K.; Fowler, M.; Ouyang, M.; Burke, A. F. Battery Safety: Fault Diagnosis from Laboratory to Real World. *J. Power Sources* **2024**, *598*, No. 234111.
(150) Sun, H.; Liang, P.; Zhu, G.; Hung, W. H.; Li, Y.-Y.; Tai, H.-C.; Huang, C.-L.; Li, J.; Meng, Y.; Angell, M.; Wang, C.-A.; Dai, H. A High-Performance Potassium Metal Battery Using Safe Ionic Liquid Electrolyte. *Proc. Natl. Acad. Sci. U.S.A.* **2020**, *117* (45), 27847−27853.
(151) Liu, J.; Bao, Z.; Cui, Y.; Dufek, E. J.; Goodenough, J. B.; Khalifah, P.; Li, Q.; Liaw, B. Y.; Liu, P.; Manthiram, A.; Meng, Y. S.; Subramanian, V. R.; Toney, M. F.; Viswanathan, V. V.; Whittingham, M. S.; Xiao, J.; Xu, W.; Yang, J.; Yang, X.-Q.; Zhang, J.-G. Pathways for Practical High-Energy Long-Cycling Lithium Metal Batteries. *Nat. Energy* **2019**, *4* (3), 180−186.
(152) Tang, M.; Dong, S.; Wang, J.; Cheng, L.; Zhu, Q.; Li, Y.; Yang, X.; Guo, L.; Wang, H. Low-Temperature Anode-Free Potassium Metal Batteries. *Nat. Commun.* **2023**, *14* (1), No. 6006.
(153) Innocenti, A.; Beringer, S.; Passerini, S. Cost and Performance Analysis as a Valuable Tool for Battery Material Research. *Nat. Rev. Mater.* **2024**, *9* (5), 347−357.
(154) Cheng, A. L.; Fuchs, E. R. H.; Karplus, V. J.; Michalek, J. J. Electric Vehicle Battery Chemistry Affects Supply Chain Disruption Vulnerabilities. *Nat. Commun.* **2024**, *15* (1), No. 2143.
(155) Qiao, W.; Zhang, R.; Wen, Y.; Wang, X.; Wang, Z.; Tang, G.; Liu, M.; Kang, H.; Said, Z.; Hwang, J.-Y.; Liu, C. Green Solvents in Battery Recycling: Status and Challenges. *J. Mater. Chem. A* **2024**, *12* (19), 11235−11265.
(156) Gervillié-Mouravieff, C.; Bao, W.; Steingart, D. A.; Meng, Y. S. Non-Destructive Characterization Techniques for Battery Performance and Life-Cycle Assessment. *Nat. Rev. Electr. Eng.* **2024**, *1* (8), 547−558.
(157) Wilkinson, M. D.; Dumontier, M.; Aalbersberg, I. J.; Appleton, G.; Axton, M.; Baak, A.; Blomberg, N.; Boiten, J.-W.; da Silva Santos, L. B.; Bourne, P. E.; Bouwman, J.; Brookes, A. J.; Clark, T.; Crosas, M.; Dillo, I.; Dumon, O.; Edmunds, S.; Evelo, C. T.; Finkers, R.; Gonzalez-Beltran, A.; Gray, A. J. G.; Groth, P.; Goble, C.; Grethe, J. S.; Heringa, J.; t Hoen, P. A. C.; Hooft, R.; Kuhn, T.; Kok, R.; Kok, J.; Lusher, S. J.; Martone, M. E.; Mons, A.; Packer, A. L.; Persson, B.; Rocca-Serra, P.; Roos, M.; van Schaik, R.; Sansone, S.-A.; Schultes, E.; Sengstag, T.; Slater, T.; Strawn, G.; Swertz, M. A.; Thompson, M.; van der Lei, J.; van Mulligen, E.; Velterop, J.; Waagmeester, A.; Wittenburg, P.; Wolstencroft, K.; Zhao, J.; Mons, B. The FAIR Guiding Principles for Scientific Data Management and Stewardship. *Sci. Data* **2016**, *3* (1), No. 160018.
(158) Greenhalgh, E. S.; Nguyen, S.; Asp, L. E.; Bici, A.; Bismarck, A.; Fam, D.; Johansson, M.; Lindbergh, G.; Lutkenhaus, J. L.; Shaffer, M. S. P.; Shirshova, N.; Srinivasan, M.; Xu, J.; Zenkert, D. Characterization and Reporting Protocols for Structural Power Composites: A Perspective. *Adv. Energy Mater.* **2025**, No. e04702.

https://doi.org/10.1021/acsaem.5c02661
ACS Appl. Energy Mater. XXXX, XXX, XXX−XXX